ELSEVIER

Contents lists available at ScienceDirect

Journal of Power Sources

journal homepage: www.elsevier.com/locate/jpowsour



Review article

Silicon oxides for Li-ion battery anode applications: Toward long-term cycling stability

Check for updates

Maziar Ashuri*, Qianran He, Leon L. Shaw

Department of Mechanical, Materials and Aerospace Engineering, Illinois Institute of Technology, Chicago, IL, 60616, USA

HIGHLIGHTS

- Silicon oxides show less volume change and a more stable cycle life than Si.
- Engineered voids can provide space to accommodate the volume expansion of SiOx.
- · Conformal carbon coating offers improved electronic conductivity of anodes.
- Strategies to overcome the problems of silicon oxide anodes are reviewed.
- Capacity fading mechanisms of different types of silicon oxide anode are summarized.

ARTICLE INFO

Keywords: Silicon oxides Prelithiation Initial coulombic efficiency Solid electrolyte layer

ABSTRACT

The emergence of developing new anode materials for Li-ion batteries has motivated experts to screen several materials to replace conventional carbonaceous anodes. Silicon oxides with different silicon and oxygen contents are a promising family of anode materials without the severe volume change of silicon-based anodes. The formation of lithium oxide and lithium silicates in the first cycle helps to buffer the volume change, while the generated amorphous silicon can secure the high specific capacity in long-term cycling. Silicon monoxide (SiO) and silicon dioxide (SiO₂) are commercially available, while silicon sub-oxides (SiO_x) are usually formed during the heating process. However, the low conductivity and poor initial Coulombic efficiency problems still exist. This review paper is focused on the strategies proposed to overcome the mentioned problems faced by silicon oxides. Based on the latest advancements, future research directions and promising methods to overcome the remaining challenges are discussed to stimulate further discussion and ideas in the rational design of silicon oxide anodes with high specific capacity and long cycle stability in the near future.

1. Introduction

Silicon with low voltage profile and high theoretical capacity (3590 mA h g $^{-1}$ for Li $_{15}$ Si $_{4}$ phase at room temperature) has been evaluated as the next generation Li-ion battery anode material in the past two decades. However, until now it cannot be employed in the practical batteries as the main active material. This is mainly due to the enormous volume change (~300%) during lithiation/delithiation processes, low intrinsic electrical conductivity, low initial Coulombic efficiency, and instability of the solid electrolyte interphase (SEI) [1–4]. The large volume change can result in particle pulverization, loss of electrical contact with the conductive additive or current collector, and even peeling off from the current collector. The repeated volume expansion

and shrinkage also lead to fracture and re-formation of the SEI layer around the particles, resulting in continuous consumption of the electrolyte, increased impedance, and capacity fading [1,2,5–9]. To overcome the issues accompanied with silicon, considerable strategies have been proposed including down-sizing the silicon materials to nanoscale, coating silicon with conductive elements such as carbon, gold, silver, and copper, trapping silicon particles inside a rigid matrix, and providing engineered space to accommodate volume change by tailored structures such as core/shell and yolk/shell designs [10–13]. Although some of these efforts ended up with promising electrochemical results, there is still a long way to see silicon as the main active material in practical application.

Due to the problems associated with silicon as anode material, the

E-mail address: mashuri@hawk.iit.edu (M. Ashuri).

 $^{^{\}ast}$ Corresponding author.

oxide form of this element has gained a huge attention recently [14–18]. This is because of the fact that during the first lithiation cycle, both lithium oxide and lithium silicate compounds form. These compounds have the ability to buffer the volume change in the successive cycles. Furthermore, many approaches that have already been tested on silicon-based anode materials are applicable to silicon oxides to overcome the intrinsic low conductivity and mild volume change of this family of materials. Here, our goal is to provide scientific insights into the lithiation/delithiation of different silicon oxides along with proposing new strategies to synthesize silicon oxide-based anodes with high potential of mass production. Based on the literature cited in this review, we are positive about utilization of this new family of anode materials for Li-ion batteries in the near future.

2. Silicon monoxide (SiO)

2.1. Chemical structure and lithiation mechanism

Silicon monoxide (SiO) is the simplest member of the silicon oxides. Its simple structure has been the subject of debates. One group of scientists believes Si–Si and Si–O bonds are distributed in the single-phase SiO material randomly (random-bonding model) [15]. In contrast, the other group postulates that SiO contains random mixture of amorphous silicon and amorphous SiO₂ phases at nanoscale level. These phases are separated by boundary regions with the 3–4 nm thickness. The interphase region dominates 20–25% of entire composition (random-mixture model) [16,19].

When compared with Si anodes, SiO experiences less volume change (less than 200% volume change), which leads to a more durable cycle life. The activation energy (Ea) of SiO for the charge process is extremely low and thus the kinetics of alloying is fast. Furthermore, the value of Ea does not depend on the type of electrolyte [20]. Because of the inhomogeneity in SiO, the lithiation of the amorphous phases and boundary layers resulted in the formation of different Li-containing products [21]. During the first lithiation of SiO, lithium oxide (Li₂O) and different forms of lithium silicates (phyllo (Li₂Si₂O₅), ino (Li₂Si₂O₃) and neso (Li₄SiO₄)) irreversibly form, which are proven to act as buffer zone to alleviate volume change. In addition, the Si-O bond is twice stronger than Si-Si, which improves the performance of SiO. However, the conductivity of SiO is extremely poor (about 10⁻¹² S cm⁻¹). The lithiation of SiO is associated with several Li⁺ consuming reactions, which affect the prediction of the theoretical capacity of SiO. Equations (1)–(3) summarize the electrochemical reactions that can occur during lithiation. Based on the proposed reactions, the delivered capacity may fluctuate between 1700 and 2400 mA h g^{-1} .

$$SiO + 2Li = Li_2O + Si \tag{1}$$

$$4SiO + 4Li = Li_4SiO_4 + 3Si \tag{2}$$

$$4Si + 15Li = Li_{15}Si_4 (3)$$

X-ray photoelectron spectroscopy (XPS) analysis revealed that the lithiation/delithiation process of SiO is associated with change in the valence of silicon from +2 to 0. Furthermore, at the charged state, 40% of Li inventory alloys with Si, while the other 60% Li transforms to Li₂O and different lithium silicate compounds. In the discharge state, the Li–Si alloy releases only 50% of its Li content and the other half remains in the alloy. The amount of lithium releases from lithium silicate and lithium oxide is very small [22].

The capacity loss of SiO at different cycles is affected by several factors. At the early stage, the incomplete delithiation because of electrode's volume change is dominated. In contrast, the capacity loss after a large number of cycles is derived from the loss of active material. The electrode composition and the ratio between the active material and binder/carbon black network are decisive for optimal performance. It is reported that by removal of defects from the interphase boundaries and

disadvantageous surface functional groups, the capacity loss can be suppressed substantially [23].

2.2. Prelithiation strategies

Prelithiation has been studied as an immediate method to increase initial Coulombic efficiency (ICE) and compensate for lithium consumption in the first formation cycle of full-cells. Furthermore, prelithiation raises the electrical conductivity and amends cycle stability of the anodes. Prelithiated anodes can pair with lithium-free cathode materials, potentially. So far, the main prelithiation strategies are grouped as electrochemical, chemical, usage of lithiated active materials, and direct contact with lithium metal [24-28]. Each route has its own pros and cons. The key point to accomplish a successful prelithiation is to control the degree of prelithiation. A variety of prelithiation reagents have been added to both anodes and cathodes including stabilized lithium metal powder (SLMP) [29], lithium silicide [30], Li₂S [31], Li₅FeO₄ [32], and Li₃N [33,34]. Among these reagents, SLMP is very promising. However, the dispersion of SLMP in toluene is not very stable. Huang et al. [29] manipulated SLMP in combination with styrene butadiene rubber (SBR) in toluene solvent. The mixture is stable and abbreviated as SST. By controlling the volume of SST, different degrees of prelithiation are attained with the ICE values ranging from 66 to 120%. However, use of SLMP requires stringent environment such as an Ar-filled glovebox to avoid oxidation of Li metal powder after SLMP has been activated. This requirement imposes some challenges or additional consideration in utilizing industry-scale dry rooms for production of SLMP-prelithiated silicon oxide anodes.

Seong et al. [35] introduced the lithium-pre-doped carbon-coated SiO composite anodes. Natural graphite and SiO were milled together with the same weight ratio for 30 min at 1200 rpm. The primary function of graphite layer (30-60 nm thick) is to increase the overall electrical conductivity. The powder after milling was utilized for electrode preparation. The casted electrode was coated with lithium. To facilitate the reaction of lithium with electrode material, the electrode was soaked in electrolyte for 24 h. After soaking, the electrode was dried at 60 °C for 48 h. The excess lithium powder and electrolyte salt were washed away with dimethyl carbonate (DMC). Based on X-ray diffraction (XRD) measurements, both lithium oxide and lithium silicate phases are produced during the pre-doping process. The pre-doping boosts up the initial Coulombic efficiency to 72.8% compared to 67.7% for the sample without Li-doping. The open circuit voltage (OCV) of the pre-doped sample was 1.84 V, while for the control sample was 3.15 V. The effectiveness of Li pre-doping was due to the artificial formation of lithium oxide and lithium silicate phase. The authors found out only 35% of lithium reacted with the active material. Therefore, additional experiments are required to exploit more lithium.

Zhao et al. [36] mechanically stirred SiO nanoparticles in molten Li for one day inside an Ar-filled glove box. The final product was a composite with Li₂O as a matrix and homogeneously dispersed Li_xSi as a secondary phase (Li_xSi/Li₂O composite). The material performed very well in both half-cell and full-cell configurations with notable upgrade in the Coulombic efficiency at the first cycle. A double layer anode (DLA) was designed by Seong et al. [37,38] to skip the chemical reaction step. The emulsified lithium droplets were casted on a copper current collector, while actual anode slurry, composed of carbon-coated SiO and polyvinylidene fluoride (PVDF) in NMP solvent, was coated on a copper mesh. The copper mesh and foil were welded together to provide the electrical path between the mesh and foil. The Li-coated foil acts as a reservoir of lithium for the anode during the cycling process. The cell fabricated with DLA demonstrates almost 100% initial Coulombic efficiency in contrast to the cell fabricated with monolayer anode (MLA) with only 55% Coulombic efficiency in the first cycle. This design ameliorates the capacity decay rate, too; while discharge capacity of MLA dropped to 402 mA h g⁻¹ after 20 cycles at 0.1 mA cm⁻² current density, the delivered capacity by DLA reached to 710 mA h g⁻¹ under

the same conditions as MLA. The shortage of Li source in the subsequent cycles is the main reason for capacity decay for DLA. This physical stacking of Li source and SiO electrode can be a rival to conventional prelithiation techniques. However, determination of sufficient loading of Li is critical. Scanning electron microscopy (SEM) uncovered the total consumption of Li after 10 cycles (Fig. 1).

Considering the fact that lithium silicate (Li₄SiO₄) and lithium oxide (Li₂O) phases are procreated in the first cycle and consume significant amount of lithium ion inventory, the irreversible capacity can raise up to 45% and therefore the ICE drops dramatically. Veluchamy et al. [39] pursued to form these compounds in the first stage. Equal moles of commercial SiO and LiOH·H₂O were heated to 550 °C for 3 h in Ar atmosphere. As a result, LiOH is decomposed to Li₂O which further reacts with SiO to form Li₄SiO₄. The product was further ball-milled with graphite for 15 h. The final product, (SiO + LiOH)/C, contains smooth and glassy Li₄SiO₄ without any traces of Li₂O. Mechanical milling reduced the particles size without forming any new phases. Lithium silicate facilitates the diffusion of Li $^+$ ions and therefore a discharge capacity of 333 mA h g $^{-1}$ after 100 cycles was acquired.

In another attempt, the reduced silicon phase is dispersed uniformly in a matrix containing the irreversible phases formed through solid-state reaction of SiO and Li at elevated temperatures [40]. Different weight ratios of SiO and Li powders are mixed with homogenizer for 1 h followed by heating at 600 °C for 2 h in Ar gas. After the reaction, reduced Si, Li₂SiO₃ and Li₄SiO₄ phases are formed. The best performance with the highest retention ratio after 15 cycles was obtained with the SiO to Li weight ratio of 7:1. This is due to the sufficient amount of Li to react with SiO. The key parameter is the homogenous dispersion of reduced Si in the matrix. Any deviation from the ideal dispersion can result in the small product size or isolation of some products without playing their

buffering role and finally capacity loss.

2.3. Carbon coating and blending with conductive materials

SiO decomposes after heating at elevated temperatures through the disproportionation process and produces Si and SiO2. This feature inspired the researchers to produce a composite of SiO with a conductive matrix such as epoxy resin, oleic acid, pitch, etc. It is demonstrated that by introducing some other chemicals, the final composite is prelithiated as well [41,42]. In one study [43], SiO powder was milled for 12 h under argon (Ar) atmosphere and coated with polyvinyl alcohol (PVA). The pyrolysis at 900 °C for 2 h, resulted in the partial disproportionation of SiO to Si, which was identified in the XRD pattern. Some SiC was formed which was not reactive to Li. The SiO/C composite cycled successfully for 100 cycles without remarkable decay (reversible capacity of more than 700 mA h g⁻¹ at 0.1 A g⁻¹ current density). However, the pure SiO sample decayed after 20 cycles. The milling helped to ameliorate the mechanical stability of electrodes, while the carbon derived from PVA promoted the conductivity of SiO. In the other experiment [44], SiO was ball-milled with graphite with different milling durations. It was shown that with increasing the milling time, the SiO became smaller in size and after 30 h milling, the material became completely amorphous without the evolution of any new alloys. Only the graphite peak intensity decays. The best composite was the one after 24 h milling. This can be due to the ideal size of the particles for Li ion diffusion.

Carbonaceous materials in composite with SiO are able to pyramid the electronic conductivity and devour the volume change. For instance, SiO/C/Graphite composite constructed by the incorporation of asphalt and graphite sheets exhibited 950 mA h g $^{-1}$ over 100 cycles at 0.1 A g $^{-1}$ [45]. Another breakthrough was achieved by nitrogen-doped carbon

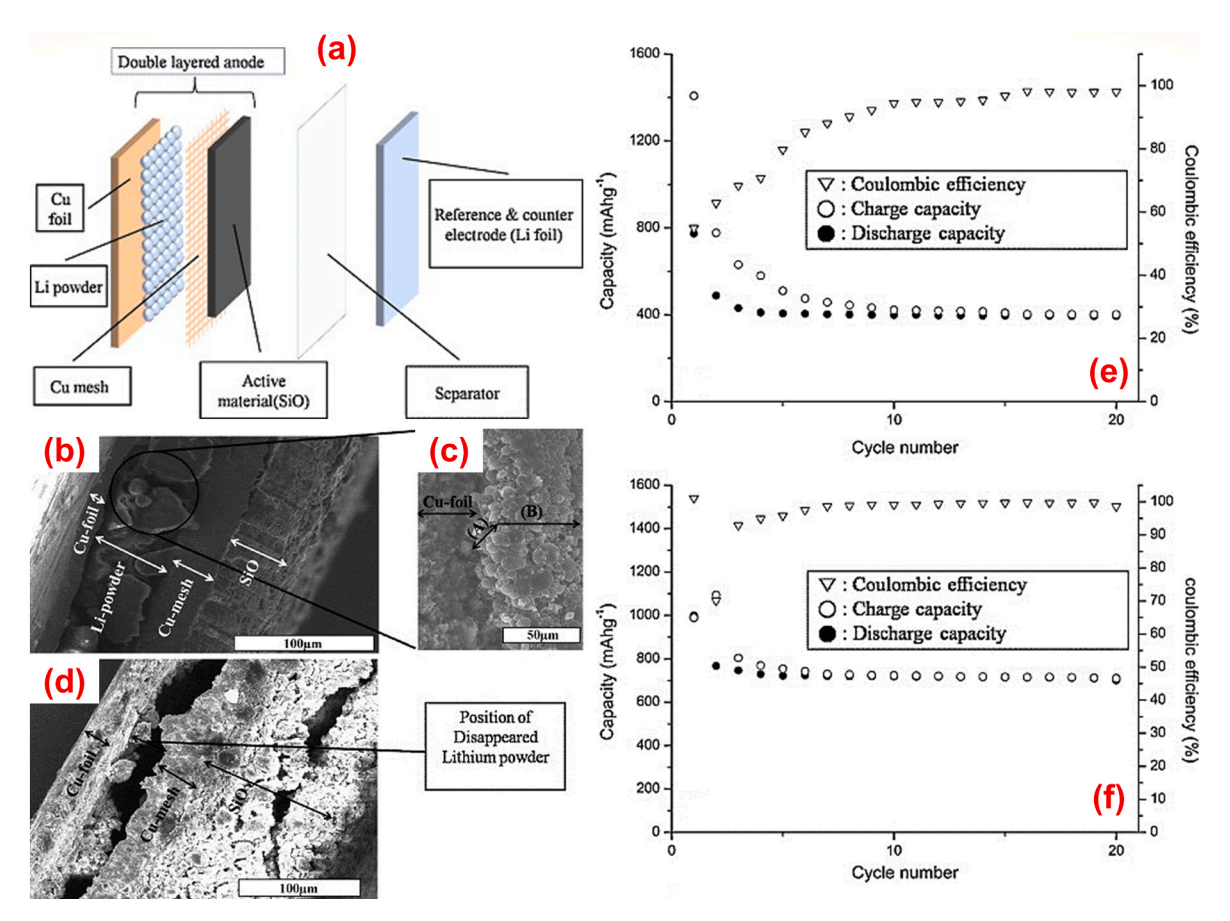


Fig. 1. (a) Schematic of the coin cell fabricated with DLA and Li metal as both reference and counter electrode, (b) SEM image of DLA before cycling, (c) magnified Li reservoir of DLA before cycling, (d) cross section of DLA after 10 cycles, capacity, and Coulombic efficiency profiles of (e) MLA and (f) DLA. Reproduced and reprinted with permission from Elsevier [37].

coating on SiO, here referred as NC-SiO [46]. The source of the carbon was an ionic liquid, named as 1-ethyl-3-methylimidazolium dicynamide (EMI-DCA). Micron-size SiO particles were dispersed in the ionic liquid followed by pyrolysis under Ar gas. From four-point probe measurement, the NC-SiO resistivity was reported as $1.3~{\rm m}\Omega~{\rm cm}^{-2}$, compared to $3.5~{\rm m}\Omega~{\rm cm}^{-2}$ for the sucrose-coated sample. Both rate capability and reversible capacity of NC-SiO were far better than bare SiO and sucrose-coated SiO. Following this idea, another group exploited dopamine as the carbon source [47]. The dopamine has the benefit of self-polymerization with a full coverage on the surface of SiO particles. The dopamine-derived conductive shell around SiO particles serves as a cushion to alleviate the volume change caused by successive cycling.

Graphene and graphene oxide (GO) are also tested in composite with SiO. The high electrical conductivity of graphene and its good mechanical stability, which can also provide buffer medium, make this material attractive. In one study [48], the milled SiO particles and graphene oxide were mixed in ethanol and subjected to hydrothermal treatment at 180 °C for 4 h. After cooling to room temperature, the powder was calcined at 675 °C under flow of Ar/H₂ mixture. To remove the SiO₂ shell, the powder was washed with 20 wt % HF acid solution. The final product was a composite consisting of SiO particles dispersed in the reduced graphene oxide (rGO) matrix. At 0.1C rate, the composite delivered 744 mA h g $^{-1}$ after 50 cycles. The good cycling performance of F–SiO/H-rGO was related to the complete wrapping of SiO particles by graphene sheets along with its better conductivity. The removal of the surface oxide layer is critical since it improved the Li $^+$ ions kinetics significantly.

To shed light on the lithiation/delithiation behavior of SiO/C, Kim et al. [49] performed a fundamental study. The carbon-coated SiO powder was utilized as active material in the cell fabrication without any conductive carbon additives. The carbon coating with approximate thickness of 40 nm was introduced by CVD technique. The delivered capacity was increased until the 14th cycle and then it started to decrease. This behavior was tracked with differential capacity (dQ dV⁻¹) curves. Two peaks observed at 0.21 and 0.06 V were associated with the lithiation, while the delithiation peaks were located at 0.31 and 0.48 V before the 14th cycle. After the 14th cycle, another peak was observed at 0.46 V in the delithiation section. This new peak is allocated to the delithiation of crystalline phase Li₁₅Si₄. As it has been mentioned before, in the first cycle, the SiO2 domains in SiO react with Li and because of this reaction, Si, Li₂O and Li₄SiO₄ form. Among these phases, only Si is active, and the rest do not react reversibly with Li in the further cycles. The complete lithiation of Si in the subsequent cycles, which leads to the formation of Li₁₅Si₄ phase at room temperature, takes time as it is confirmed by XRD. The lithiation of Si in the early stage causes the volume expansion and formation of cracks in the particles. This increased contact area between electrode and electrolyte provides easier Li ⁺ ions diffusion and more lithiation of the Si. The lithiation of silicon to a complete lithiated phase is a gradual process. The delithiation of Li₁₅Si₄ is a reversible process in the first few cycles. However, after 100 cycles, this phase was observed in the XRD pattern. This is an indication of the presence of some isolated Si particles, which were not able to perform lithiation/delithiation reversibly and as a result, the capacity decayed over 100 cycles.

To further overcome the low intrinsic electronic conductivity of SiO and structural damage caused by volume change, Cu deposition followed by carbon coating treatment have been applied to SiO. Zhang et al. [50] formulated a composite of SiO with electroless-deposited copper and expanded graphite (EG). The copper improves the electrical conductivity, while the flexible EG abolishes the cycling stress. Besides this role, EG grants the appropriate wettability of the electrolyte which is particularly important to maintain the ionic conductivity. The main source of stress developed in the SiO/Cu/EG composite is the alloying between silicon and lithium. It is worth mentioning that based on the Eqs. (1)–(3), after the first cycle, the active material is limited to the amorphous silicon. The real-time stress measurement indicates that

the stress developed in SiO/Cu/EG electrode is much lower (23 MPa) than both bare SiO (70 MPa) and SiO/Cu electrodes (65 MPa). The findings emphasized the importance of the EG as a critical component of the structure. The synergistic effects of about 13% copper content and role of EG to ameliorate the cycling stress helped the SiO/Cu/EG composite delivers about 800 mA h g⁻¹ after 100 cycles at 0.2 A g⁻¹ rate. In the other experiment by this group [51], Cu nanoparticles are deposited on SiO particles via a galvanic displacement reaction followed by exposing the SiO/Cu particles to sucrose solution followed by heating at 800 °C for 3 h to produce SiO/Cu/C composite. An initial capacity of 1140 mA h g⁻¹ and a reversible capacity of 1006 mA h g⁻¹ at 100 mA g⁻¹ over 150 cycles are related to the cooperative functions of the deposited Cu nanoparticles and amorphous carbon layer. Copper nanoparticles cannot stand the structural stress introduced to the materials during cycling and it is crucial to add an amorphous layer to slightly mitigate the volume change.

2.4. Doping with other elements

Doping with different elements is caried out to further aggrandize the performance of SiO. For the boron (B) doping, spin-on dopants (SOD) method is utilized [52]. The elemental B is coated on a p-type silicon wafer and placed above the SiO containing crucible. The heat treatment was performed under the flow of nitrogen gas at 900 °C for 3 h. At 900 °C, the disproportionation reaction was triggered with the final product of silicon nanoparticles dispersed in the amorphous SiO_x matrix. The presence of boron caused the distortion in silicon and consequently, silicon Raman peak was shifted from 508 to 498 cm⁻¹. Likewise, the lattice constant of silicon was slightly reduced due to the effect of doping element. The doped sample exhibited higher delivered capacity and rate retention compared to both bare specimen and the SiO sample heat treated at 900 °C without any doping (reversible capacity of about 1000 mA h g⁻¹ after 100 cycles at 0.5C rate). Doping with B has lowered the charge transfer resistance of SiO electrodes. It also facilitated the diffusion of Li⁺ ions; the diffusion coefficient of doped sample was reported as $4.25 \times 10^{-11} \text{ cm}^2 \text{ s}^{-1}$, compared to $9.28 \times 10^{-12} \text{ cm}^2 \text{ s}^{-1}$ and $3.34 \times 10^{-12} \text{ cm}^2 \text{ s}^{-1}$ for un-doped heat-treated and bare SiO, respectively. The results obtained with B doping proved that SiO can function as anode material even without carbon coating.

Another recommended dopant is red phosphorus (P) [53]. It is proven that P can form bonds with oxygen of SiO and carbon derived from carbon source (here anthracite), and therefore red P joined SiO and carbon together to provide stable structure. The embodiment of red P caused the disorder characteristic of carbon coating to become more pronounced; the I_D/I_G intensity ratio was increased to 2.52 based on the Raman spectroscopy. It is accepted that formation of more defects and vacancies in the structure is in favor of Li $^+$ ion storage. The introduction of red P in the SiO/C composites increased the initial Coulombic efficiency, discharge capacity and capacity retention. It is worth to mention that due to the presence of P in the structure, the SEI layer formation was expedited which helps to improve the initial Coulombic efficiency. The impedance analysis of half-cells after soaking confirmed the reduction of charge transfer resistance after red P incorporation, which is surprising since P is an insulator (Fig. 2).

2.5. Composite with metal oxides

Zirconium oxide (ZrO_2) is assessed as a second phase in SiO/ZrO_2 composites [54]. It is introduced by the high-energy planetary ball milling with zirconia balls inside a zirconia jar for 10 h. The incomplete-crystallized tetragonal phase of ZrO_2 acts as a buffer layer to relieve the volume changes of SiO, while the conductivity is enhanced through the formation of ca. 5 nm thick carbon coating by constant pressure chemical vapor deposition of carbon (acetylene gas used as carbon precursor). The short annealing time at 800 °C (only 20 min) guarantees the formation of D and G bands in the Raman spectra without

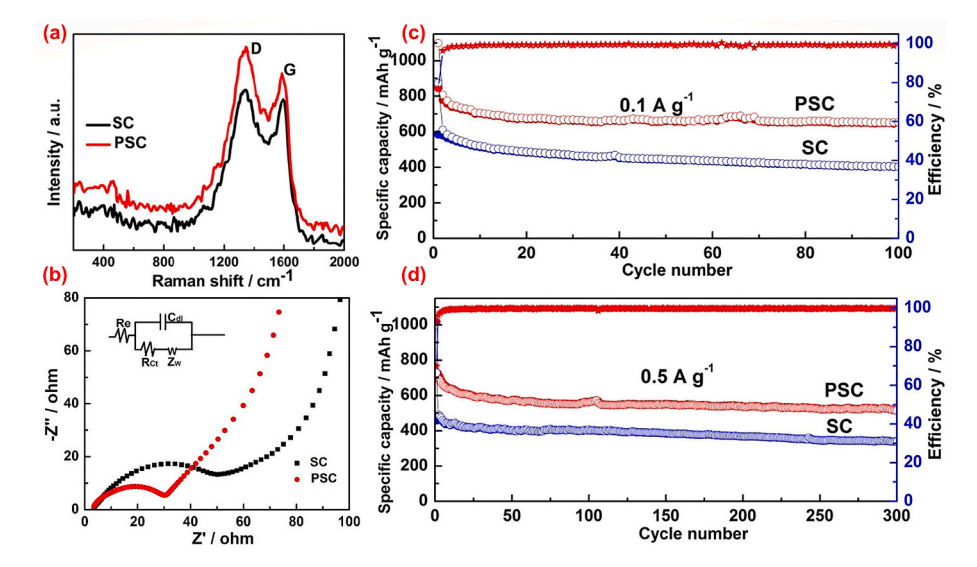


Fig. 2. (a) Raman spectra of SiO/C composites (SC) and phosphorous-modified SiO/C composite (PSC), (b) EIS curves for SC and PSC half-cells, 300 charge/discharge cycles of SC and PSC half-cells at (c) 0.1 and (d) 0.5 A g⁻¹ current densities. Reproduced and reprinted with permission from Elsevier [53].

evolution of new phases in the end product. The amorphous carbon-coated SiO/ZrO $_2$ composite performed much better than as-received SiO and ball-milled SiO. The SiO/ZrO $_2$ composites successfully were cycled for 100 cycles at 0.8 A g $^{-1}$ current density delivering about 700 mA h g $^{-1}$. They also showed decent rate capability at different current rates.

3. Silicon dioxide (SiO2)

3.1. Chemical structure and lithiation mechanism

Silicon dioxide (SiO₂) with the theoretical capacity of 1950 mA h g^{-1} , moderate volume change (100%), and inexpensive mass production (due to its abundance on earth crust) is a strong candidate to replace silicon as anode material [17,55]. The lithiation of silica provokes both reversible and irreversible reactions to produce silicon, lithium oxide and lithium silicates. All reactions are exothermic and exergonic [56]. Lithium silicates help the formation of a stable SEI layer, while Li₂O absorbs the volume change associated with lithiation to some extent. Despite these benefits, the consumption of lithium causes the decrease in energy density and ICE. The electronic conductivity of SiO2 is low and it experiences a significant volume change during lithiation. Due to these complications, researchers have pursued different paths to boost its electrochemical performance using the techniques such as surface coating with carbon and other oxides, downsizing the particle size, embedding silica in an elastic matrix, providing extra space with hollow nanostructures, prelithiating with different agents, etc.

Mesoporous silica nanospheres are synthesized in large scale with controlled narrow size distribution through sol-gel route. In most cases, tetraethyl orthosilicate (TEOS) is used as the main precursor to form silica. However, the usage of TEOS is limited for industrial applications because of its toxicity and flammability. After hydrolysis and condensation at different pH values, concentrations, and temperatures, amorphous silica nanospheres with uniform size distribution are produced [57,58]. Tu et al. [59] prepared the ${\rm SiO}_2$ nanospheres with average diameter of 400 nm and utilized them as an active material. The capacity decreased at the first few cycles, but gradually increased in the following cycles. This is related to the diffusion of Li ions and observed in other studies. The battery survived after 500 cycles delivering about 900 mA h g $^{-1}$ capacity, which is comparable to other designs especially hollow spheres.

3.2. Carbon coating and blending with conductive materials

Coating silica with carbon is a pragmatic means to tackle the intrinsic poor conductivity of SiO₂, not to mention that the carbon component ameliorates the structural integrity. Based on the major phase, the hybrid composites are named as silica/carbon [60,61] or carbon/silica composites [62-64]. The carbon is introduced as a coating with certain porosity [65] and/or as a confining element for silica, i.e. graphene or carbon nanotubes [66-72]. Depending on the carbon source and how it is utilized, different microstructures are accomplished. Addition of some other conductive elements such as titanium oxide (TiO₂), nickel oxide (NiO), iron monosilicide (FeSi) and copper can advance the overall properties of the composites and speed up the interfacial charge transfer reactions [73-76]. In one study [77], nano-sized SiO2 particles were hydrothermally coated with sugar followed by carbonization at 1000 °C. The obtained HC-SiO₂ composite powder was tested electrochemically and exhibited stable cycling performance. The authors affirmed that smaller silica particles tended to be reduced to silicon and lithium oxide (Li₂O), while the larger particles formed Li₄SiO₄ along with Si in the first discharge. In another experiment [78], SiO₂ nanoparticles soaked in the sucrose solution and then carbonized at 900 °C under nitrogen atmosphere to produce a carbon coating. This composite material has a good lithium storage capacity (500 mA h g⁻¹ after 50 cycles). The carbon coating decreases the interfacial resistance. Similar to previous study [77], both the nano-size effect of SiO₂ and the irreversible formation of Li₂O and Li₄SiO₄ at the first discharge, are the main reasons for the good electrochemical performance of the composite. Xia et al. [79] have dispersed the nano-sized ultra-fine silicon dioxide particles in a mixture of glucose and sodium citrate. Through the hydrothermal synthesis, a very uniform solution obtained. The solution was centrifuged, and the collected powder was subject to pyrolysis at 800 °C under nitrogen atmosphere. The SiO₂/C composite has a surface area of 186 m² g⁻¹ with average 4 nm pore size. The composite delivered the reversible capacity of about 500 mA h g⁻¹ after 100 cycles at 0.1 A g⁻¹ current density. Recently, a ternary composite of silicon dioxide nanoparticles, graphene, and multi-walled carbon nanotubes (MWCNTs) has been evaluated as anode material. Uniform suspension has been achieved through ultra-sonication. The silica nanospheres were enclosed in the carbon network completely, which provided the good cycle life [80].

Lv et al. [81], ball-milled silica with sucrose and carbonized the mixture at 900 °C under N_2 atmosphere. The SiO_2/C composite had exceptional capacity compared to the similar composite without introduction of mechanical milling (600 mA h g⁻¹ compared to 100 mA h g⁻¹

after 100 cycles at 0.1 A g $^{-1}$ rate). In the sample prepared without milling, plenty of domains of crystalline SiO $_2$ (3–10 nm in size) were observed in the amorphous matrix. However, the mechanically milled sample had no crystalline domains with the change in the SiO $_2$ bond length and angle. The distorted structure paved the way for Li $^+$ ions diffusion to the composite structure, while the amorphous carbon layer prevents the aggregation of SiO $_2$ particles during cycling along with its role to improve the conductivity of the entire structure.

Nanoscale SiO_2 is evaluated in composite with 3D porous carbon matrix [82]. The tailored architecture obtained with two precursors including Na_2SiO_3 as silica source and glucose as carbon source. Sodium Chloride (NaCl) was employed as a templating agent. After dissolving all chemicals in distilled water, the solution was heated until a dark brown powder remains in the beaker. The solution crystallized around the NaCl template, and the crystalline particles were coated uniformly with glucose. The powder was carbonized at 650 °C for 2 h. Then the powder submerged in HCl to convert Na_2SiO_3 to H_2SiO_3 . Further heating at 170 °C resulted in decomposition of H_2SiO_3 to SiO_2 and H_2O (Equations 4) and (5)).

$$Na_2SiO_3 + 2HCl \rightarrow 2NaCl + H_2SiO_3 \downarrow$$
 (4)

$$H_2SiO_3 \xrightarrow{170\,^{\circ}C} SiO_2 + H_2O \uparrow \tag{5}$$

Thermogravimetric analysis revealed the presence of 78 wt percent of carbon in the final product. SEM observations proved the uniform dispersion of SiO_2 nanoparticles in the sub-micron carbon matrix. The composite illustrated promising performance at high rates (187.4 mA h g⁻¹ at 5 A g⁻¹). Long term cycling of the composite was reported at 0.1 A g⁻¹ rate and at this rate, the reversible discharge capacity of 434 mA h g⁻¹ was gained after 50 cycles [82].

3.3. Hollow silica nanostructures

Hollow silica nanospheres with bridged organic functional groups are proven to be an effective nanostructure for energy storage materials. They possess unique features such as low density, high surface area, and superior mechanical and thermal stability. However, the synthesis of this well-tuned nanomaterials is challenging. Sasidharan et al. [83,84] adopted ABC triblock copolymer micelles with core-shell-corona architecture as template. These templates were utilized in both alkaline and acidic media. The precursor of the inorganic compound is adsorbed on the corona layer, and after the polymerization reaction is finished, they form the shell of the desired hollow nanospheres. The core removal process is executed either by solvent extraction or calcination methods and it leaves voids inside the nanostructure. In one experiment [83], the triblock copolymer of poly(styrene-b-2-vinyl pyridine-b-ethylene oxide) (PS-PVP-PEO) was adopted as a template and tetramethoxysilane (TMOS) as the silica reagent. After calcination, the spheres shrunk to the 30% of their original volume. The uniform and small grain size of the spheres (30 nm) as well as optimized cavities in the hollow structure resulted in a reversible capacity of 400 mA h g⁻¹ after 500 cycles. Poly (styrene-b-[3-(methacryloylamino)propyl]trimethylammonium chloride-b-ethylene oxide) (PS-PMAPTAC-PEO) was also tested by this group [84]. After the addition of bis[3-(triethoxysilyl)propyl]disulfide (BTDS, 96%), the precursor for silicon, and aging reaction at 100 °C for 48 h, a crystalline benzene-silica hollow nanosphere was procreated. With the assistance of the PS-PMAPTAC-PEO micelle, the shell was charged with the quaternary ammonium cation groups and thus, the micelles can function at any pH. The benzene-silica nanoparticles as anode preserve durable capacity up to 300 cycles at 1C. Another innovative approach in hollow core-shell silica particles, is multi-shell hollow silica microspheres (MHSM) [85]. The amount of sodium silicate (Na₂SiO₃) adsorbed into the template, carbonaceous microspheres (CMSs), is the key to increase the shell numbers of hollow SiO2 from 1 to 3. This directly affects the quantity of metasilicic acid (H₂SiO₃) produced after hydrolysis.

In the calcination step, the CMS material is burnt while the adsorbed $\rm H_2SiO_3$ transformed to $\rm SiO_2$ nano-building blocks. The growth of the outer $\rm SiO_2$ layers is accelerated because of their exposure to higher temperatures. The smaller inner silica nanoparticles are gradually in favor of the larger particles due to the Ostwald ripening phenomenon. MHSMs functioned prominently as anode active materials (reversible capacity of 750 mA h g $^{-1}$ after 500 cycles at 100 mA g $^{-1}$ for MHSM with three silica shells).

Hollow silica spheres with carbon coating not only minimize the Li⁺ ions diffusion pathways, but also the so-called "buffer zone" indemnifies the volume change of active materials. One parameter in choosing the carbon source for coating is the number of nitrogen-containing groups available in the carbon source. After carbonization reaction, they leave a N-doped carbon with some defects in the carbon structure. As a result. the diffusion of Li⁺ ions across the interface becomes faster. Xiao et al. [86] clearly elucidated the difference between the resorcinol formaldehyde (RF) and polydopamine by applying them on the same hollow SiO₂ nanospheres. The sample coated with polydopamine showcased higher capacity and better stability compared to the one coated with RF. Kim et al. [87] attained the composite nanostructure via chelation of silicon tetrachloride (SiCl₄) by citric acid in 1,2-dimethoxyethane (glyme) solvent, followed by carbonization at 900 °C for 1 h. The citric acid acts as both chelating agent and carbon source. The carbon content was reported as 4.2 wt %. The cycling performance and rate capability of this material was far better than commercial nano-SiO₂, about 91% capacity retention after 100 cycles.

Taking advantage of sacrificial templates to synthesize hollow nanostructures is a popular technique. The template materials are a variety of polymer nanoparticles such as PS, PVA, PAA, etc. with uniform shape and size distribution. The silica shell is applied by the sol-gel reaction. The removal of the template is done either by leaching or heating at elevated temperatures. Cao et al. [88] tried to embed the silica sphere in a porous carbon matrix. They started with PS nanospheres (average diameter of 200 nm) as a sacrificial template and formed the silica layer around them by the addition of TEOS. After removal of PS, hollow spheres were mixed with both resol and triblock copolymer P123. By carbonization of this precursor, hollow silica spheres embedded in porous carbon (HSS–C) were produced. This composite has a high surface area (297 m 2 g $^{-1}$). The eminent performance of this nanocomposite (910 mA h g $^{-1}$ after 150 cycles at 0.2 A g $^{-1}$ rate) is due to the porous carbon matrix, which acts as a continuous conductive network to facilitate the Li ions movement and alleviate the volume change during alloving/dealloving. Liu et al. [89] coated silica around polyacrylic acid (PAA) nanoparticles to generate hollow spheres with uniform shell thickness of 35 nm. Sucrose used as a carbon source and after it was carbonized at 800 °C for 2 h, the carbon shell formed around the hollow spheres. The carbon film connects all the spheres together, and in the meantime diminishes the resistance of the nanostructure. Different silica loading was examined. It turned out that the sample with 67 wt % SiO₂ had the best performance among other specimens (650 mA h g⁻¹ after 160 cycles). The charge/discharge process initiates the crack formation in some nanospheres, which is the main failure mechanism in long term. Exploiting two different carbon sources was explored by Jiao et al. [90]. First, SiO₂/PVA microspheres were fabricated by aerosol spraying. Then, a thin layer of polyacrylonitrile (PAN) was applied on the surface of the microspheres. Finally, annealing at 800 °C creates SiO₂@po-C@C composites. After 100 cycles at 100 mA g^{-1} , a capacity of 669.8 mA h g^{-1} was reached. The inner porous carbon skeleton established a highway for Li $^{\mathrm{+}}$ ions transfer inside the structure at high rates and the PAN-based outer shell promoted a stable SEI layer.

Self-assembly is another method to prepare hollow nanomaterials. For instance, hollow SiO_2 spheres with about 135 nm shell thickness are prepared with this technique [91]. In the next step, a PAN-derived carbon layer is applied to the spheres, and eventually micron-level H–SiO₂/C particles with the reversible capacity of 600 mA h g⁻¹ after

400 cycles are realized. The carbon layer functions as a mechanical support to ensure longer cycling stability (Fig. 3).

Despite the fact that the hollow nanospheres are the preferred concept for SiO_2 , other nanoarchitectures such as hollow nanotubes [92] and hollow nanocubes [93] are also promising with the capability to convey similar performance and stability. The common synthesis route for these specific nanostructures is a two-step hard-templating process and removal of the template in the last step. For SiO_2 nanotubes, anodic aluminum oxide (AAO) templates are heated at 650 °C with polydimethylsiloxane (PDMS) as SiO_2 precursor and the silica vapor completely covered the AAO template. Phosphoric acid (H₃PO₄, 50 wt %) is used to dissolve the AAO completely. The very thin walls of SiO_2 nanotubes grant the high utilization of active material and aid the fast movement of Li $^+$ ions at high rates.

3.4. Silica from natural abundant resources

Natural resources of silica such as desert sand, rice husks and etc. have attracted vast attention in case of large scale production of silica and silicon [94]. One of the amplest chemical compounds in the earth's crust is Quartz (SiO2). To make it reactive with Li, high energy mechanical milling (HEMM) with the charge ratio of 20 to 1 was employed [95]. The material becomes amorphous with broad XRD peaks as the milling time increases. It is worth mentioning that the amorphization starts after 12 h milling time and it is completely amorphous after 24 h milling. The sample after 24 h milling was selected for battery fabrication. The reversible capacity delivered after 200 cycles was reported as 800 mA h g^{-1} with the retention 80%. It is proven that the addition of 15 wt % Al could improve the low initial Coulombic efficiency up to 50%. Detailed HRTEM investigation revealed that amorphous silicon dioxide (a-SiO₂) went through the following reactions (Equations (6)-(10)) at the mentioned voltages during the first charge/discharge process. The reversible formation of both Li₁₅Si₄ and Li₂Si₂O₅ phases at discharge and their decomposition to Si and SiO2 in the charge were observed in the further cycles. This lithium insertion mechanism is similar for the nanostructured silica thin films deposited by reactive radio frequency sputtering [96].

$$a - SiO_2 + \frac{4}{5}Li^+ + \frac{4}{5}e^{-\frac{discharge\ to\ 0.27\ V}{5}} + \frac{2}{5}Li_2Si_2O_5 + \frac{1}{5}Si$$
 (6)

$$a - SiO_2 + 2Li^+ + 2e^- \xrightarrow{discharge \ to \ 0.24 \ V} \frac{1}{2}Li_4SiO_4 + \frac{1}{2}Si$$
 (7)

$$Si + \frac{15}{4}Li^{+} + \frac{15}{4}e^{-\frac{discharge \text{ to } 0.0 \text{ V}}{4}} + \frac{1}{4}Li_{15}Si_{4}$$
 (8)

$$Li_{15}Si_4 \xrightarrow{charge \ to \ 0.34 \ V} 15Li^+ + 4Si + 15e^-$$
 (9)

$$Li_2Si_2O_5 + \frac{1}{2}Si \xrightarrow{charge to 0.39 \ V} \frac{5}{2}SiO_2 + 2Li^+ + 2e^-$$
 (10)

Kubuqi desert (Inner Mongolia, China) sand has also been evaluated as a natural silica source [97]. Since the particle size of the sand is large (about 300 µm), planetary milling was exploited to reduce its size. Since the sand contains several metal silicates as impurities, after milling the powder was washed with HCl for 24 h. The milling time directly affects the size and lithium storage properties of the anode material. Planetary milling was done under Ar atmosphere with the ball to powder ratio of 50:1 at constant 500 rpm speed for 36, 60, 72 and 108 h. The average particle sizes were reduced from 1.835 µm for 36 h to 446 nm for 108 h milling. By decreasing the particles size, both peak broadening and some peaks disappearance phenomena were observed in both XRD patterns and FTIR spectra, which is common for materials subjected to mechanical milling process. As the particle size decreased, the delivered capacity increased, which is the sign of a better utilization of active material. The 72 h milled sample delivered about 400 mA h $\rm g^{-1}$ capacity over 400 cycles with the capacity retention of about 95%. The milling produced numerous lattice defects along with increase in the specific surface area. The synergistic effects of these phenomena made the silica more electrochemically active. Furthermore, the first lithiation caused the formation of lithium silicate and lithium oxide which acted like buffer medium. Moreover, the metal silicates impurities and the portion of silica, which remained inactive, aided to attenuate the volume change of anode material during the charge/discharge process. This simple and low cost method has opened a new window in the large scale production of anode materials with high specific capacity.

Rice husks is a common waste of agricultural industries with a production of more than 600 million tons a year. Its major components are silica and hydrocarbons such as lignin, cellulose, and hemicellulose. The silica absorbed by rice during its growth is in the form of silicic acid. The silica in the rice husks is nanoscale and agglomerates close to cellulose compounds [98]. Heating the rice husks at elevated temperatures under an inert atmosphere provokes the organics to decompose and leave a porous carbon matrix bearing a homogenous dispersion of silica nanoparticles (10–50 nm). This simple treatment creates C/SiO₂ composites with a reversible discharge capacity of 485 mA h g⁻¹ after 84 cycles [99]. To further induce porosity, zinc chloride (ZnCl₂), as an activating agent, is employed to dissolve cellulose and leaves pore. ZnCl₂ does not react with silica, and it is removed easily from the structure through washing with 0.5 M HCl solution. To find out the optimum carbonization temperature, Cui et al. [100] investigated the temperature range of

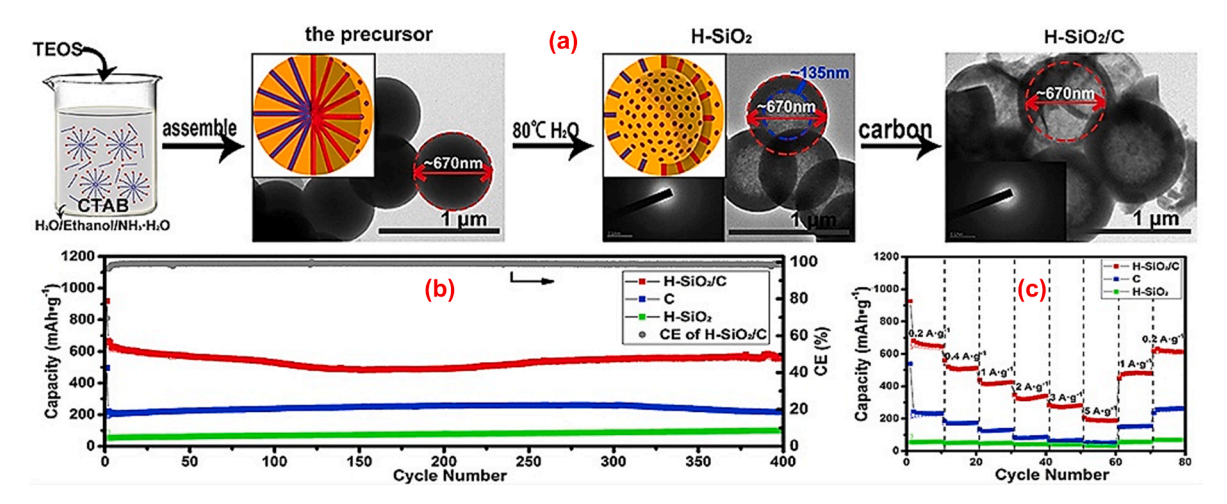


Fig. 3. (a) Synthesis steps of H–SiO₂/C nanospheres, (b) long-term cycling performance at a current density of 200 mA g^{-1} , and (c) capacity retention at different current densities for H–SiO₂, carbon, and H–SiO₂/C electrodes. Reproduced and reprinted with permission from Elsevier [91].

 $500-650\,^{\circ}\text{C}$. The increase in the temperature increases the share of SiO_2 over C. Both specific surface area and pore volume increased with rising temperature up to $600\,^{\circ}\text{C}$ (1191.30 $\text{m}^2\,\text{g}^{-1}$ and $0.396\,\text{cm}^3\,\text{g}^{-1}$), but these values decreased at $650\,^{\circ}\text{C}$. The cell fabricated using the specimen prepared at $600\,^{\circ}\text{C}$ displayed the highest discharge capacity of $1105\,\text{mA}$ h g^{-1} at $0.1\,\text{A}\,\text{g}^{-1}$ and best cycling stability with little fading over $360\,\text{cycles}$. This exceptional performance is in debt of the highly porous C/SiO_2 nanostructure with uniform distribution of silica without aggregation plus the increased conductivity provided by disordered carbon. This carbon layer can also relieve the volume change of SiO_2 nanoparticles during lithiation/delithiation (Fig. 4).

Rice husk ashes (RHAs) incorporates 92–95% silica nanoparticles along with alkali metal oxides in amorphous carbon. In order to put them to use, a surface activation by hydrogen peroxide (H₂O₂) is carried out [101]. After removal of alkali metal oxides by washing with HCl, the RHAs were exposed to H₂O₂ at 100 °C followed by drying at different temperatures varying from 200 to 800 °C under flow of Ar gas. The increase in heating temperature resulted in removal of more carbon. Therefore, the optimum drying temperature was set as 200 °C. The surface modification results in the propagation of mesopores inside the structure of RHAs along with the increase in surface roughness. The first cycle discharge capacity of RHA is 580 mA h g⁻¹, while the first discharge capacity of surface-modified RHAs can be varied between 870 and 1227 mA h g⁻¹ depending on drying temperature. This simple surface treatment can make a new window in the area of biomass utilization.

4. Non-stoichiometric silicon oxides (SiOx)

4.1. Chemical structure and lithiation mechanism

Non-stoichiometric silicon oxides (or silicon sub-oxides) with a general formula of SiO_x are also explored as Li-ion battery anodes. The oxygen content can be varied, but all compositions are reactive to lithium. There is a trade-off between the silicon and oxygen content in SiO_x -based anodes. The higher silicon content results in higher capacity

and ICE, while the cycling stability is not promising [15,102]. By increasing the oxygen content, the amounts of lithium oxides and lithium silicates formed after the first lithiation increase, and therefore the voltage hysteresis advances. In one of the earliest studies [55], three different compositions and four sizes are selected and tested: SiO $_{0.8}$ (50 nm), SiO (2 μ m), and SiO $_{1.1}$ (30 and 50 nm). All of them alloyed with lithium metal reversibly with and without the usage of solvent for slurry (here the solvent used was NMP). Among them, SiO $_{0.8}$ displayed remarkable capacity. Furthermore, particles with smaller size have slower capacity decay during cycling.

Generally speaking, SiOx is amorphous and thermodynamically unstable. Thus, during carbon coating or atomic doping, which usually involve high energy mechanical milling or heating at elevated temperature or both, disproportionation reaction occurs easily. This differentiates between the electrochemical performance of bare SiO_x and the disproportionated SiOx, both of which are worthy of systematic investigation [103]. Two sets of specimens were prepared; in one batch SiO_x particles were first milled and then heated at elevated temperature (denoted as M - H), while in the other set, annealing was first performed and then the sample was milled (denoted as H-M). These samples showed different performances. While annealing above 950 °C provokes disproportionation, it also results in the formation of an insulating O-rich SiO₂ layer on the surface of the particles, which blocks the Li⁺ ions pathway. This layer can be easily broken by mechanical milling. As a result, SiO_x is activated, the charge impedance is reduced, and the reaction kinetics becomes faster. High-energy mechanical milling (HEMM) was applied to the commercially available SiO_x particles [104]. The milling was carried out in a zirconia jar with zirconia balls for 10 h. The particle size reduced from several microns to about 1 µm after milling. Furthermore, an amorphous phase covered the surface of the particles. The milled powder was collected and used as active material for battery fabrication. After the first lithiation, both Li₂O and Li₄SiO₄ compounds were formed which helped to gentle the volume expansion during cycling. The reported capacities are much higher than the raw SiO_x starting material.

Implementing sufficient pores in the structure of the electrode

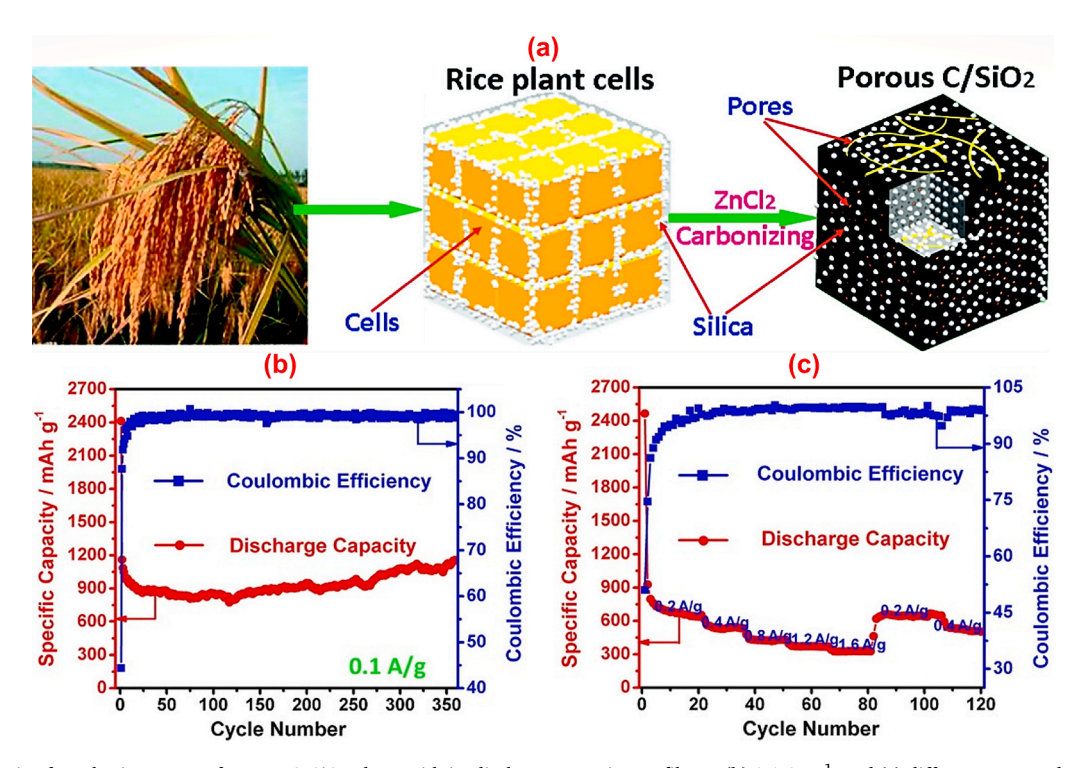


Fig. 4. (a) Schematic of synthesis process of porous C/SiO₂ along with its discharge capacity profiles at (b) 0.1 A g⁻¹, and (c) different current densities. Reproduced and reprinted with permission from Elsevier [100].

materials is critical since the pores are channels for the Li⁺ ions transport. However, reaching the appropriate pore size and distribution is not an easy task. Yu et al. [105] developed a novel approach based on the etching of silicon. They started with the bulk SiO particles (\sim 325 mesh). After heating at 900 °C, the disproportionation reaction occurred, and crystalline silicon nanoparticles embedded inside the amorphous silicon oxides (SiO_x) matrix. The mechanical milling under inert atmosphere helped to reduce the particles size and made the distribution of nano-silicon zones more uniform. The last step to achieve the porous structure was etching with 1 M NaOH solution for 4 h at room temperature. The key to success in this step was the significant etching rates of nano-silicon zones and the SiO_x matrix. Since the crystalline silicon zones dissolve faster in the solution, they are considered as pore generating agents. The final product showed up to 105.41 m² g⁻¹ surface area while the milled product's surface area was only 19.57 m 2 g $^{-1}$. The fabricated anodes delivered a stable capacity of 1240 mA h $\rm g^{-1}$ after 100 cycles at 0.2C rate. The rate capability of this material was excellent. This method does not require working with strong acids such as HF and has the potential of being commercialized. Furthermore, there is no carbon coating step, which simplifies the process and makes it more attractive for industrial applications.

4.2. Hollow SiO_x nanostructures

Hollow porous structured ${\rm SiO}_x$ coated with two layers of carbon (DC-HSiO_x) was investigated by Xu et al. [106]. The first carbon layer was derived from calcination of phenolic resin at 900 °C for 3 h under the Ar atmosphere, while the second layer contains the spray-dried graphene oxide sheets which are then reduced to graphene oxide (rGO) at elevated temperatures. The hollow structure provides short diffusion paths for Li⁺ ions and the carbon skeleton improve the conductivity and mechanical robustness during cycling. The presence of the 3D rGO network is essential, since the amorphous carbon is not able to withstand the volume expansion of silicon oxide for a large number of cycles. This fact is highlighted by evaluating the single amorphous carbon coated-HSiO_x (HSiO_x/C) vs. DC-HSiO_x.

Yolk-shell structure is an another promising design for both silicon and silicon oxides, since it provides enough void space to buffer the huge volume expansion. However, yolk-shell structured electrodes usually collapse after repetitive charging/discharge cycles. This is mostly due to the fact that the shell is not thick enough. One solution to increase their lifetime was proposed by Liu et al. [107]. A three-layer SCN-SiO₂@CH₂CH-SiO₂@SH-SiO₂ microspheres were synthesized by sol-gel reaction. The interlayer was selectively etched by sodium hydroxide solution and then, the SCN-SiO2@void@SH-SiO2 microspheres were annealed at 800 °C for 5 h under Ar atmosphere to carbonize all organic groups and form a yolk-shell SiO_x/C particles. A semi-graphitic carbon layer was deposited on both internal and external surfaces by CVD technique. The SiO_x/C-CVD composite delivered 972 mA h g⁻¹ at 0.5 A g⁻¹ after 500 cycles in half cell. The full cell built by this material and lithium cobalt oxide (LiCoO2) as cathode obtained a reversible capacity of 137 mA h g⁻¹ at 0.1C after 100 cycles. The CVD-induced semi-graphitic carbon coating not only improved the electrical conductivity of the yolk-shell, but also enhanced its structural integrity.

4.3. Carbon coating and blending with conductive materials

The combination of nanoscale features with the electronic conductivity of the epoxy resin-derived carbon coating has been tested to revitalize the capacity of SiO_x -based composites [108]. The starting material is the silica obtained through modified Stöber method. Epoxy resin has been added to the solution under vigorous stirring to form a gel. The gel carbonized at 650 °C under air. TEM observations uncovered that the $\mathrm{SiO}_x/\mathrm{C}$ nanoparticles contain well-ordered domains, which matches with SiO_2 plane spacing, and disordered domains, which are amorphous Si clusters. The ordered domains are active to Li and their

alloying reaction results in the irreversible formation of $\rm Li_2O$ and $\rm Li_4SiO_4$, which buffer the drastic volume change. It is worth mentioning that a vast amount of $\rm Li^+$ ions are consumed to form these compounds and that is why in the initial cycles the irreversible capacity is high. The rate capability and capacity retention of this material is very good (800 mA h g $^{-1}$ after 50 cycles at 0.1 A g $^{-1}$ current density).

To achieve SiO_x/C particles with spherical morphology, a facile synthesis route based on the heating of a mixture of polydimethylsiloxane ($(SiOC_2H_6)_n$, PDMS) and hexane in a sealed vessel was developed [109]. The hexane role was to avert the agglomeration of spheres. Therefore, a homogenous dispersion of SiO_x and nanoscale carbon phase was formed. Particles with spherical morphology are stable in terms of mechanical properties and dispersed better in electrode slurry. Thus, the generated stress by the volume change of silicon oxide is more uniformly distributed across the electrode. The resultant particles demonstrated paramount delithiation capacity (1603.1 mA h g $^{-1}$ at 0.3 A g $^{-1}$ after 400 cycles) and high capacity retention.

 ${
m SiO_x/C}$ microspheres with outstanding electrochemical properties are synthesized by Liu et al. [110]. The sol-gel process with vinyltriethoxysilane (VTES) produced the uniform silica spheres and the resorcinol was employed as the carbon source. The carbon content of these spheres is tunable and depends on the amount of resorcinol varies from 20 to 60 wt %. After 400 cycles, the delivered specific capacity was reported as high as $700 \, {\rm mA} \, {\rm h \, g}^{-1}$ at $0.5 \, {\rm A \, g}^{-1}$ rate. Additionally, the rate capability is phenomenal. This achievement is attributed to the uniform dispersion of ${\rm SiO_x}$ nano-domains in the carbon matrix. The carbon is not crystalline, acts as a highway for electron passage, and maintains the integrity of the structure after the expansion. The authors paired this anode with commercial LiFePO₄ cathode and proved its functionality in full cell.

Many scientists are inspired to searching for carbon precursors such as glucose, dopamine, and NafionTM ionomers as the conductive phase [111–114]. In one study [114], the glucose solution is added dropwise in the modified Stöber process. When the gel is developed, it was ground with more glucose in the planetary mill for 5 h with the ball to powder ratio of 10 to 1. The powder is collected and pressed into a disc and carbonized at 950 °C for 30 min under the air atmosphere. The carbonized disc is further ground and fine powder used as active material. The composite was investigated with various analytical techniques. Based on the XRD patterns, the short heating time did not result in the formation of crystalline silicon and the powder contains the amorphous SiO_x phase dominantly. The uniform carbon layer was formed around the SiO_x core with the average thickness of 10 nm based on the energy dispersive spectroscopy (EDS) line scan measurements. The elemental analysis revealed the ratio of O to Si is about 1.9. The SiO_x/C composites showed excellent performance at both low and high current densities (674.8 mA h $\rm g^{-1}$ at 0.1 A $\rm g^{-1}$ after 100 cycles and 485 mA h $\rm g^{-1}$ at 0.5 A $\rm g^{-1}$ after 100 cycles). The addition of glucose in two separate steps (SiOx-C) is a key point and the author revealed that one-time addition of all glucose before ball milling did not end up with high performance (SiO_v-C). The carbon layer formed around the SiO_x nano-domains and the extra carbon coating around the secondary particles are the two prominent features that help to boost the properties of this composite. The ball milling aided uniform distribution of the SiO_x nano-domains and prevented agglomeration. The first lithiation products including Li₂O and Li₄SiO₄ helped to harness the volume change, while the carbon coating provided excellent conductivity and blocking electrolyte (Fig. 5).

Dopamine contains functional groups such as catechol and amines and can easily polymerize in an alkaline medium. After being pyrolyzed at elevated temperatures, it leaves nitrogen-doped carbon coating. The incorporation of nitrogen in carbon improves the electronic conductivity and thus electrochemical performance of $\mathrm{SiO}_x/\mathrm{C}$ nanocomposites. In one attempt [115], the N-doped carbon shell around SiO_x core increased the reversible capacity to 1514 mA h g⁻¹ after 100 cycles at 100 mA g⁻¹. This progress is ascribed to the superior conductivity of the N-doped

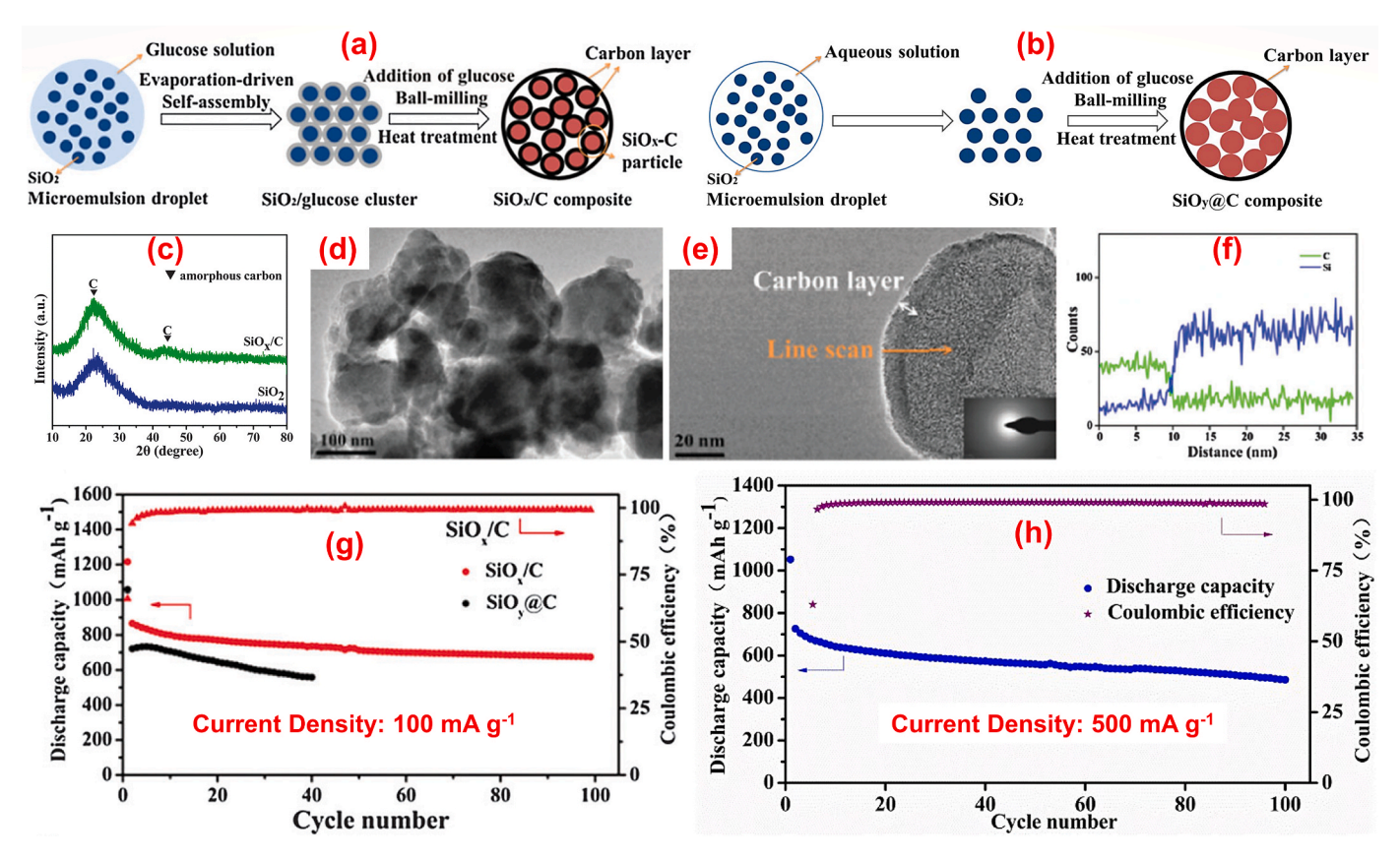


Fig. 5. (a) Schematic of the two-step addition of glucose synthesis, (b) addition of all glucose before ball milling, (c) XRD pattern of SiO_x /C composite, (d) TEM, (e) HRTEM, (f) EDS line scan, (g) discharge capacity of SiO_x -C vs. SiO_y -C composites at 0.1 A g^{-1} for 100 cycles, and (h) discharge capacity of SiO_x -C composites at 0.5 A g^{-1} for 100 cycles. Reproduced and reprinted with permission from Royal Society of Chemistry [114].

carbon layer as well as its role in mitigating the SiO_{x} volume change in repeated cycling.

The oxidation degree (x) of silicon plays a key role in reversible capacity and long-term cycling stability of SiO_x -based materials. The lower x value translates to higher discharge capacity. This fact has inspired researchers to replace TEOS with ethyltriethoxysilanes (EtSi(OEt)_3) as precursor [116]. Resorcinol/formaldehyde (RF) was utilized as a carbon source which participated in a sol-gel reaction with polysiloxane in the presence of cetyltrimethylammonium bromide (CTAB) as surfactant in alkaline medium. Annealing at 1000 °C under the Ar atmosphere produced sugar apple-shaped $SiO_x@C$ nanocomposite spheres. The discharge capacity of 563 mA h g $^{-1}$ at the rate of 100 mA g $^{-1}$ after 400 cycles made $SiO_x@C$ nanospheres an ideal electrode material. The durability of this material is assigned to its nanoscale feature along with unique spherical morphology and porosity, which caused the homogenous dispersion of SiO_x in disordered carbon.

Following the previous study [116], $SiO_x@C$ composites were synthesized in the form of the one-dimensional nanorods to overcome the poor conductivity of SiO_x along with its volume change during lithiation [117]. The carbon coating with resorcinol yields about 34.6 wt % carbon after annealing at $1000\,^{\circ}C$ for 3 h. The TEM observations unveiled that nanorods formed contain so many nanospheres connected inside the rod in a preferred orientation to harness the mechanical induced stress. The EDS analysis showed the uniform distribution of silicon, oxygen, and carbon elements with the approximate value of x as 1.12 in SiO_x formula. The cycling performance of the $SiO_x@C$ nanorods at 0.1 A g⁻¹ showed significant discharge capacity of about 720 mA h g⁻¹ after 350 cycles. The rate capability of the $SiO_x@C$ nanorods at different current rates was substantial, too. At $0.05\,$ A g⁻¹ rate, the discharge capacity was as high as 770 mA h g⁻¹ and when the current density increased to 0.8 mA g⁻¹, the discharge capacity was set as 410 mA h g⁻¹. After reverting

the rate back to 0.05 A g $^{-1}$ rate, the composite retained the capacity of 775 mA h g $^{-1}$. The excellent properties root from the one-dimensional design of the nanorods which shortens the lithium ion diffusion path along with the improved conductivity SiO_x , which is derived from carbon coating. The influence of the carbon coating is highlighted in the EIS spectra. The diameter of the semicircle part of the EIS curve was reduced to about 60% of the sample without carbon coating. The interconnected nanorods with the facile synthesis steps can be one of the promising designs for the future Li-ion battery anodes with high performance.

To overcome the poor conductivity of SiOx, multiwall carbon nanotubes (MWCNTs) are incorporated to build up a conductive scaffold and anchoring site for SiO_x [118]. In order to improve contact between them, an N-doped carbon layer derived from polyacrylonitrile (PAN) was introduced to achieve SiOx/MWCNT/N-doped C ternary composite. As expected, a stable reversible capacity of $620 \text{ mA} \text{ h g}^{-1}$ at a current rate of 100 mA h g⁻¹ was achieved over 450 cycles. The initial Coulombic efficiency was also improved to 60.6%. Conductive MWCNT combined with the N-doped carbon layer prevents the agglomeration of SiO_v particles, as well as shortening the diffusion pathways of both electrons and Li⁺ ions. Graphene nanoplatelets (GNPs) are another conductive additive that are exploited. GNPs with diameters ranging from 0.5 to 25 μm and thickness of 5–25 nm have been explored in catalysts, sensors, supercapacitors, etc. To take advantage of GNPs in SiOx, a self-assembly approach followed by a high temperature heating approach was chosen to prepare SiO_x-C/GNPs [119]. The silicon source was C₂H₅Si(OC₂H5)₃ (denoted as EtSi(OEt)3) and the silicate oligomers, and GNPs were bound together with the aid of CTAB and aqueous ammonia. After heating at 1000 °C for 3 h, all organic molecules decomposed, and SiO_x-C film anchored on GNPs. This GNP supported composite delivered a stable reversible capacity of 630 mA h g⁻¹ at 100 mA g⁻¹ after 250 cycles. Such a good performance results from the dramatic increase in

conductivity of SiO_x -C after anchorage on GNPs along with the elastomeric nature of GNPs which helps to hold the SiO_x particles together during volume expansion and prevent crack formation or pulverization of electrodes.

The performance of SiO_x/C nanocomposites is further amplified by chromium (Cr) coating [120]. The carbon coating was accomplished by the ball milling of silicon monoxide and graphite, while the Cr coating was applied through ion beam sputtering on the surface of the SiO_x/C nanocomposite electrode. The Cr layer was uniform with the thickness of 40-50 nm. The coated material tested in the full cell configuration with lithium cobalt oxide as cathode. The initial capacity of nanocomposites increased from 684 mA h $\rm g^{-1}$ to 690 mA h $\rm g^{-1}$ at 0.1C rate. When the material becomes more conductive, it can collect more Li⁺ ions with faster transfer rate. The capacity retention of the Cr-coated samples was revamped compared to the uncoated sample from 69% to 75% for 100 cycles. The electrode with Cr coating kept the initial morphology after several cycles, while the uncoated electrode material completely reacted with electrolyte and bulged remarkably. The coating has multiple benefits: enhance the electrical conductivity, increase the adherence of active materials to the substrate, and improve the mechanical properties to harness the volume change of silicon monoxide.

4.4. Doping with other elements

To improve the reversible capacity and rate capability of SiO_x anodes, boron (B) is introduced in the microstructure through calcination at $500\,^{\circ}\text{C}$; a multielement, multiphase B-doped SiO_x is produced [121]. Lithium borohydride (LiBH₄) was mixed with SiO and upon heating, amorphous B, B_2O_3 and nanocrystalline Li_2SiO_3 were formed mostly on the surface. The presence of B and B_2O_3 advanced both elastic modulus and hardness. Besides, they aided to form a more stable SEI layer and suppressed the volume change of SiO_x . The half-cells fabricated from $SiO-0.3LiBH_4$ mixture showed a reversible specific capacity of 940 mA h g $^{-1}$ after 200 cycles.

4.5. Prelithiation strategies

To overcome the problem of ubiquitous lithium consumption in the first cycle, Li coating on separator is explored [122]. The Li slurry was prepared by dissolution of lithium and PVDF in triethyl phosphate (TEP) solvent. The weight ratio of Li to PVDF was 10:1 and the slurry was casted on one side of a polypropylene (PP) separator followed by drying. The coating thickness was reported as 100 µm with 0.5 mg cm⁻² of Li loading. The Li-coated separator was pressed to the anode composed of SiO_x and graphite ball-milled together for 30 min at 1200 rpm (SiO_x-C). The cathode used in this experiment was LiCoO₂. The Li in the separator acts as a reservoir to improve the discharge capacity in the first cycle along with boosting the initial Coulombic efficiency of the cell from 66.4% to 88.8%. The results are promising, however there is still more than 10% irreversible capacity loss. Hence, testing different loadings of Li is necessary to track its effects. The findings clearly showed that up to 0.5 mg cm⁻² of Li loading, the improvement in both of the mentioned factors is noticeable. However, increasing the loading did not cause any improvement. Therefore, $0.5~\text{mg}~\text{cm}^{-2}$ was set as the saturation limit for Li loading. The Li not only reacts with SiOx-C to produce the buffer compounds such as Li₂O and Li₄SiO₄, but also participates in some side reactions including SEI layer formation, Li plating on the anode after a few cycles, and overcharging of the anode. This recipe is also implemented on silicon and graphite anodes and in both cases remarkable enhancements were achieved.

4.6. Large-scale production of SiO_x

Many routes are proposed to prepare the non-stoichiometric silicon oxides. A group of Korean scientists developed a novel method to control the oxidation of molten silicon [123,124]. High purity SiO_x

nanoparticles with various oxidation states ranging from 1.18 to 1.83 were obtained by blowing the mixture of oxygen and argon gas to molten silicon. The $\rm O_2/Ar$ ratio controls the degree of oxidation (x) and also the color of the final product. At low x-values, a crystalline Si phase was detected, showing a higher capacity but faster capacity decay, which is caused by the pulverization of the crystalline Si phase. When x-value exceeds 1.28, the crystalline Si disappeared, and amorphous $\rm SiO_x$ was detected. Besides, at high x-value the number of nanoparticles increased, the cycle performance is much stable than commercial $\rm SiO_x$, due to more nanostructure and more oxide buffer formation around the Si. However, the initial reversible capacity decreases, when x-value is high due to a large amount of Li-based oxide formation consuming Li-ions. When $\rm x=1.18$, nano-SiO_x is able to deliver 660 mA h g⁻¹ reversible capacity after 50 cycles, while reaching the Coulombic efficiency of 99.8%.

The reduction of silicon dioxide (SiO₂) with magnesium metal (Mg) can yield silicon oxide (SiO_x) with different oxidation states. There are many parameters such as temperature, uniform mixing and pore length playing a role in this process which can directly affect the lithium storage capacity of the final product. Su et al. [125] have investigated the effect of the pore length on the reduction degree of mesoporous silica precursors and found out that decrease in pore length causes the increase in the reduction degree. This phenomenon is related to the extent of diffusions of molten Mg inside the pores. The sample with the chemical formula of SiO_{0.73} was cycled for 60 cycles and delivered the reversible capacity of about 600 mA h g⁻¹. The magnesiothermic reduction process was combined with coating with two conducting materials silver and polyaniline (PANI) ended up with high-performance composite [126]. The nanopores generated in the structure are favorable for Li ions diffusion, while the conductive coating buffers the structure. Moreover, the silicon nanocrystals generated from the magnesiothermic reduction, were well-dispersed in the matrix and hold the volume changes of the composite structure together during the successive charge/discharge cycles.

During large-scale production of silicon, a sizable portion of silicon is lost during slicing ingots with wire saws. By installing appropriate glass filters in the production line, the kerf loss is collected. It consists of silicon oxides mixed with crystalline silicon and amorphous silica with bimodal particle size distribution (322.9 nm and 17.9 μ m) [127]. The particles delivered initial charge and discharge capacities of 1572.8 and 456.3 mA h g⁻¹, respectively. After 100 cycles, the discharge capacity dropped to 40.6% of the first cycle with Coulombic efficiency close to 100%. This study introduced a new environmental and economical route to recycle SiO_x particles from the silicon ingot processing waste [128].

To lower the production cost of SiO_x -based nanomaterials, researchers demonstrated a mass-productive synthesis based on low-cost siloxane [129]. It started with preparing a solution of TEOS in DI water, ethanol, and hydrochloric acid as acidic catalyst, followed by the addition of aqueous ammonia as basic catalyst to form colloidal solution. Sucrose was added prior to gelation. Sucrose-coated silica particles were ball-milled for 5 h and carbonized at 900 °C under N_2 atmosphere. Silica reacted with carbon at hot temperatures and converted to silicon sub-oxide coated with a 3–6 nm carbon layer covering the surface uniformly. Elemental analysis affirmed the O/Si as 0.88. The resultant SiO_x /C nanocomposite electrode exhibited a reversible capacity of 820 mA h g⁻¹ at 0.1 A g⁻¹ rate for 100 cycles with excellent rate performance.

4.7. SiO_x from natural abundant resources

Rice husk is an abundant source of silica which is composed of particular organic compounds. This natural resource motivated Chinese scientists to investigate its potential as anode material. In one case [130, 131], rice husks were washed thoroughly with DI water without introducing any acids and then subjected to two-step carbonization process;

the first stage involved heating at 450 °C under N₂ flow to convert rice husks into carbon precursor, while the second step was calcination at 900 °C sintering under Ar/H2 atmosphere for several hours (SiOx/C composite). The hydrogen gas flow promotes reduction of silica to silicon. The presence of low valence silicon increased the electrochemical performance, while heat treatment at 900 °C increased the carbon ordering in composite structure (graphitization). This economic filth-to-wealth utilization of rice husks yielded natural SiO_x/C composites, which exhibited discharge capacity of 600 mA h g⁻¹ at 100 mA g⁻¹ over 100 cycles. In another study [131], aluminothermic reaction at 700 °C associated with carbon coating generated SiO_x@C composite with high specific surface area (up to 600 m² g⁻¹). The excess Al₂O₃ byproducts were removed through washing with HCl. The nobility of this method is no need for an external carbon source and the carbon coating is generated by burning of rice husks. The entire method is benign with commercialization potential. The batteries cycled for 200 cycles with reversible capacity of about 1230 mA h g⁻¹ at the current rate of 0.1 A g^{-1} .

Diatomite and beach sand are natural resources for SiO2 and considered as a powerful rival to toxic silane gas in silicon and silicon oxide production. In a feasible magnesio-mechanochemical process [132], diatomite or pre-treated sand (milled for 1 h) were mixed with magnesium powder (Mg, 200 mesh) and milled inside a planetary milling machine with zirconia balls. The reduction took place, and SiO_x particles were synthesized. The byproducts of the reaction including MgO, Mg₂SiO₄, Mg₂Si, and unreacted Mg can be removed with 1 M HCl solution. The obtained SiO_x particles constitute nanoclusters of SiO₂ as well as Si enveloped by different sub-oxides. A reversible capacity of 644 mA h g⁻¹ was obtained at 4 A g⁻¹ after 2000 cycles in half-cell format (71.3% of the 3rd cycle capacity). For practical Li-ion battery applications, the SiO_x particles were blended with artificial graphite. The coin cells delivered reversible capacity of 587 mA h g^{-1} at 0.2 A g^{-1} after 200 cycles (89.7% capacity retention). This exceptional cycling performance is owed to the presence of nanoclusters of silicon distributed inside SiO_x structure and the sufficient porosity which guaranteed the successful expansion/shrinkage of silicon. The nanoscale SiO2 left in the structure was converted to Li₂O and lithium silicates in the successive charge/discharge cycles and mitigated volume expansion of silicon along with spurring the formation of a SEI layer with higher stability.

Shaddock peels contain a substantial number of cellulose fibers and are exerted as porous nitrogen-doped carbon precursors for supercapacitor and battery applications. The porous biocarbon, which has ideal electronic conductivity, can be decorated with SiO_x nanoparticles with the aid of a microwave-assisted hydrothermal process followed by pyrolysis at 900 °C for 3 h under nitrogen flow. Reversible capacity as high as 740 mA h g⁻¹ over 100 cycles under a current density of 0.358 A g⁻¹ was reported for C/SiO_x with 20.8 wt % of SiO_x. Higher loading of SiO_x nanoparticles does not necessarily lead to higher discharge capacity due to lack of rigid connection between SiO_x and biocarbon frame [133].

4.8. New Binders for SiO_x-based composites

In addition to the efforts on engineering the microstructure of SiOx, having a binder with exceptional mechanical properties is also vital. The conventional PVDF binder is not capable of managing the volume expansion of silicon-containing anodes. In one study, graphite and SiO_x particles (x \sim 0.95), both in micron size range, were mixed together in a weight ratio of 1:1 and utilized as active electrode material. The addition of graphite amplifies the conductivity of the blend and results in formation of a steadier SEI layer. Different binders including polyimide (PI), PVDF and a carboxymethyl cellulose (CMC)-based water dispersed binder (WDB) were examined in electrode fabrication. Electrochemical testing results along with both in situ and ex situ SEM verified that flexible binder (here, PI) combined with small particle size of SiO_x can meliorate both rate capability and cycling stability of the half-cells The crystallographic changes occurred during [134].

lithiation/delithiation of graphite-SiO_x blends were recorded using in situ XRD technique [135]. The anodes composed of 80 wt % graphite and 20 wt % SiO_x (x \sim 0.95). The collected XRD patterns during charge/discharge affirmed that the lithiation of graphite starts with applying current, while in case of graphite-SiO_x, the Li $^+$ ions initially insert into SiO_x and after certain time the lithiation proceeds in both SiO_x and graphite until the graphite is fully lithiated. Furthermore, during the discharge process, SiO_x delithiates later than graphite (Fig. 6). The presence of silicon oxide leads to a delayed graphite intercalation with Li⁺ ions and thus the kinetics of graphite-SiO_x becomes slower. These differences are explained by the different chemical potentials of graphite and SiO_x.

Carboxymethyl cellulose (CMC)/styrene butadiene rubber (SBR) binders can only function with silicon oxides mass loading of 3–5 wt %. Thus, researchers grafted this binder with dopamine-functionalized heparin to achieve up to 7 wt % $\rm SiO_x$ loading in graphite- $\rm SiO_x$ mixture [136]. Heparin contains various functional groups including amine and sulfonate. The amine groups in heparin react with the acid groups of CMC to construct a physical crosslinking by forming strong hydrogen bonds. The sulfonate group increases the overall $\rm Li^+$ ion conductivity of the binder. Dopamine with excellent adhesion to silicon is also grafted to heparin to improve its adhesion. The anode containing dopamine-heparin/CMC/SBR binder was tested in full-cell format vs. NMC622, and the cell retained 92% of its initial capacity after 150 cycles.

5. Summary and perspectives

The promising electrochemical performance of silicon oxides, as summarized in this review and Table 1, makes this group of materials a potential candidate for Li-ion battery anodes. However, there are still problems that need to be tackled before commercialization. Based on the review of the latest advancements in this article, the following conclusions and perspectives can be offered.

- (1) Numerous studies have shown that the intrinsic low conductivity of silicon oxides can be solved by mixing uniformly or coated with carbonaceous materials at nanoscales. Good cycle stability with high specific capacities such as 1050 mA h g $^{-1}$ after 400 cycles at 0.1 A g $^{-1}$ rate [109], 689 mA h g $^{-1}$ after 400 cycles at 0.5 A g $^{-1}$ rate [110], and 720 mA h g $^{-1}$ after 350 cycles at 0.1 A g $^{-1}$ rate [117] have been achieved with this strategy.
- (2) The large volume expansion/shrinkage problem of silicon oxides can be addressed by introduction of engineered porosity along with mixing or coated with carbonaceous materials. The former provides space to accommodate the volume expansion, whereas the latter offers electronic conductivity as well as confinement or buffering effects on the volume expansion. The works described in Refs. [107,110] by the same group illustrate nicely the effectiveness of introducing engineered porosity can improve the specific capacity and cycle stability simultaneously from 689 mA h g^{-1} after 400 cycles for SiO_x/C to 972 mA h g^{-1} after 500 cycles for yolk@shell SiOx/C. Another important work by Wu et al. [132] demonstrates convincedly that introducing meso- and micro-pores to mixed nano clusters of SiO2 and Si can lead to an anode with 644 mA h $\rm g^{-1}$ specific capacity after 2000 cycles. This work [132] is the only one that has shown more than 1000 cycle stability for SiO_x-based anodes and proven without any doubts the importance of engineered voids in achieving long-term cycle stability of SiO_x-based batteries.
- (3) In spite of the advancements mentioned above, long-term cycling data for SiO_x is lacking. In contrast, there are quite a few reports on silicon-containing materials with cycling data over 1000 cycles [3], whereas the work described in Ref. [132] is the only one demonstrating the success of SiO_x-based batteries with more than 1000 cycles. There is no doubt that such research is urgently

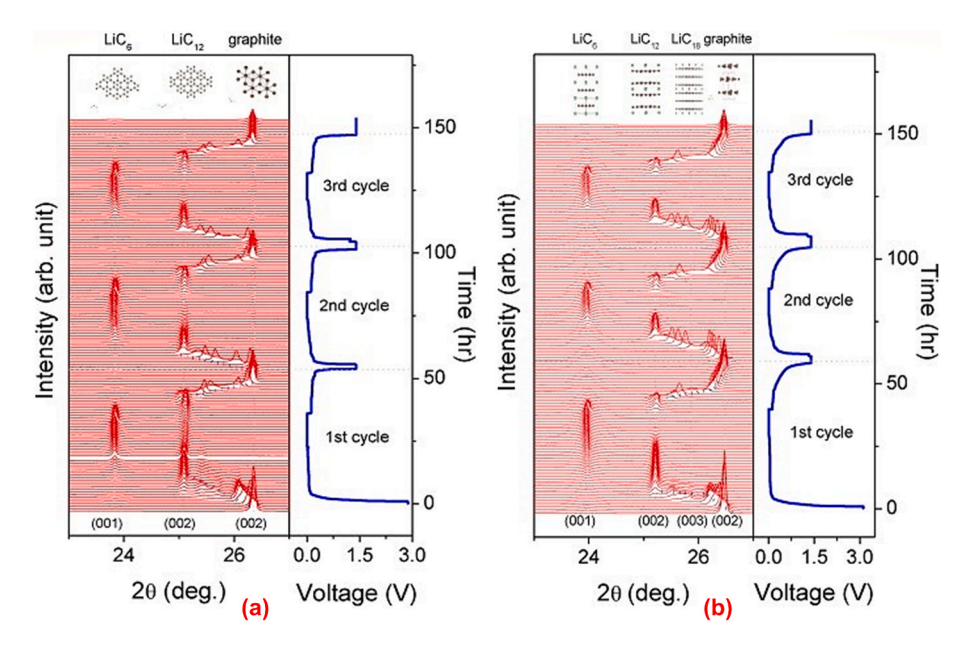


Fig. 6. Lithiation/delithiation curves and in situ XRD patterns for (a) graphite, and (b) graphite-SiO_x. Reproduced and reprinted with permission from Elsevier [135].

Table 1Comparison of electrochemical performance among a variety of silicon oxide anode materials reported in open literature.

-	•	-	-		
Silicon oxide material design	Reversible specific capacity (mA h g^{-1})	Charge/discharge cycles demonstrated	Max. charge rate (mA g^{-1})	Initial Coulombic Efficiency	Ref.
SiO-C	710	100	100	76%	[43]
NC-SiO	955	200	1500	73.9%	[46]
carbon-coated SiO/ZrO2	721	100	800	66.58%	[54]
Mesoporous SiO2 nanoparticles	1060	150	100	17.4%	[57]
H-SiO ₂ /C	638.7	400	200	69.5%	[91]
Hollow porous SiO ₂ nanocubes (HPSNCs)	919	30	100	47%	[93]
SiO_x/C	674.8	100	100	70%	[114]
SiO _x /MWCNT/N-doped Carbon	621	450	100	66%	[118]
SiO_x/C	780	100	100	61%	[139]

 Table 2

 Characterization techniques to study silicon oxide based anode materials.

Characterization Technique	Purpose	Advantage	Disadvantage
X-ray photoelectron spectroscopy (XPS)	Study the SEI layer composition and check the Si valence at different stage of charge/discharge	Obtain chemical state and empirical formula of different compounds	Better to be done at synchrotron source to generate X-rays with different intensities
X-ray absorption spectroscopy (XAS)	Study the formation of amorphous products during cycling and better understanding the degradation mechanisms	High accuracy for local environment of Si atoms data	Requires synchrotron radiation to generate X-rays with appropriate edges for different elements
In situ X-ray Diffraction (XRD)	Determine the amount of different crystalline phases during the charge/ discharge process	Easy to perform if the cycler is connected properly to XRD	Time consuming and better to be done at synchrotron source
¹ H/ ⁷ Li/ ²⁹ Si magic angle spinning Nuclear Magnetic Resonance (MAS NMR)	Detect the silicon domains in silicon oxides and identify the lithium silicates compositions	High accuracy for structural information	Expensive, time consuming, and requires many calibrations to collect meaningful data

- needed because the technical targets for EV applications are 1000 cycles with 80% capacity retention and much higher specific energy than that of graphite-based Li-ion batteries (LIBs).
- (4) Another important area that deserves investigation before one can embrace SiO_x -based batteries is the study of thick electrodes with an areal capacity reaching at least 4–5 mA h cm $^{-2}$. This areal capacity is comparable to those of commercial LIBs with graphite anodes. To achieve this areal capacity, the SiO_x mass loading should be around 5.7–7.1 mg cm $^{-2}$ for a SiO_x anode with a specific capacity of 700 mA h g $^{-1}$. These high SiO_x mass loadings per unit area could decrease significantly the specific capacities reported in most of the articles reviewed herein if the SiO_x anodes do not have high specific power. This point is well elucidated in Ref. [109] where a specific capacity of 1050 mA h g $^{-1}$ after 400 cycles for a SiO_x/C anode with a mass loading of 1.5 mg cm $^{-2}$ SiO_x/C composite is reduced to 666 mA h g $^{-1}$ for the same anode but with a mass loading of 3.0 mg cm $^{-2}$ SiO_x/C and otherwise the identical conditions. High mass loading leads to thick electrodes and thus mass transport can become a limiting factor resulting in lower specific capacities.
- (5) Another area that needs attention is the valuation of SiO_x -based anodes coupling with different cathode materials in the full-cell configuration. Up to now, the number of scientific papers containing this type of electrochemical data is very limited. One important topic in this area is the area specific capacity balance of the negative to positive electrode (N:P) ratio, which is crucial

- because it affects both energy density as well as lifetime of full cells. A recent study [137] on Si//NMC532 full cells reveals that some oversizing of Si anodes is needed for cycle life of the full cells to avoid fast decay of the Si anode. Given the similar volume expansion challenge of SiO_x anodes as Si anodes, we anticipate that the N:P ratio study will attract attention in the near future.
- (6) The low Coulombic efficiency at the first cycle is still present in many SiO_x-based designs and no effective solutions have been proposed to overcome this matter. The prelithiation is one of the most effective methods. However, it has its own obstacles. The stabilized lithium metal powder (SLMP) is widely used for this purpose, but the price of this powder is still high. Preparation of uniform slurry is another challenge, since SLMP can agglomerate and prevents the complete mixing with active material and carbon black. Thus, the distribution of SLMP in slurry after drying will not be uniform. Furthermore, the requirement of an Ar atmosphere to activate the distributed SLMP still imposes challenges in using SLMP at the industry-scale dry room manufacturing facilities. Other prelithiation methods such as short circuit and mechanical mixing in the molten lithium [138] are not as straightforward as SLMP. The need to study other prelithiating agents such as lithium nitride (Li₃N) is necessary.
- (7) Although not the focus of this review, new binders with sufficient mechanical properties have been studied in both academia and industry. Some data reported in the literature are collected with special binders, which makes the judgement on the proposed SiO_x design extremely hard. Self-healing and functionalized binders are the two new categories of binders attracted huge attention. The self-healing binder aids to overcome the volume change, while the Li-functionalized binder increases the conductivity and affinity of anode to Li⁺ ions. It is worth trying to combine these two families to obtain a binder with extraordinary properties.
- (8) New electrolyte development with the ability to form a stable SEI layer is also required. Different additives such as fluoroethylene carbonate (FEC), vinylene carbonate (VC) and vinyl ethylene carbonate (VEC) have been proposed to elevate the cyclability of Si-based anodes. However, such studies on SiO_x anodes are limited. Further, systematic studies coupled with simulation and modelling such as molecular dynamics (MD) are vital to accomplish a unique formulation for SiO_x anodes.
- (9) Detailed characterizations on SiO_x-based anodes specifically at different states of charge and at different cycles can shed light to the charge/discharge mechanisms associated with this class of material. X-ray absorption spectroscopy (XAS) studies are highly recommended because of its strength to detect amorphous species. XAS visualizes the lithium oxide formation in the first cycle. Combining this technique with in-situ and in-operando techniques can provide invaluable information Table 2.
- (10) The last but not the least, designing a scalable process to harvest silicon oxides with the desired silicon and oxygen contents from natural abundant resources such as rice husks and desert sand is a key to commercialize this family of materials. Process engineers are encouraged to focus on facility and scalability of their proposed synthesis routes. The removal of byproducts is a challenging part of the process and still requires further elevation. Usage of benign solvents to dissolve the byproduct can make the process eco-friendly. The catalysts and heat scavengers increase the yield of the process and save more time, energy, and money.

Declaration of competing interest

The authors declare that they have no known competing financial interests or personal relationships that could have appeared to influence the work reported in this paper.

Data availability

No data was used for the research described in the article.

Acknowledgements

This work was supported by the U.S. National Science Foundation (NSF) with the award numbers CMMI-1660572 and IIP-1918991. MA and LS are also grateful to the Rowe Family Endowment Fund.

References

- C.K. Chan, H. Peng, G. Liu, K. McIlwrath, X.F. Zhang, R.A. Huggins, Y. Cui, Nat. Nanotechnol. 3 (2008) 31–35.
- [2] L. Pan, H. Wang, D. Gao, S. Chen, L. Tan, L. Li, Chem. Commun. 50 (2014) 5878–5880.
- [3] M. Ashuri, Q. He, L.L. Shaw, Nanoscale 8 (2016) 74-103.
- [4] M. Obrovac, L. Krause, J. Electrochem. Soc. 154 (2007) A103-A108.
- [5] S.D. Beattie, D. Larcher, M. Morcrette, B. Simon, J.-M. Tarascon, J. Electrochem. Soc. 155 (2008) A158–A163.
- [6] M. Holzapfel, H. Buqa, L.J. Hardwick, M. Hahn, A. Würsig, W. Scheifele, P. Novák, R. Kötz, C. Veit, F.-M. Petrat, Electrochim. Acta 52 (2006) 973–978.
- [7] B. Liang, Y. Liu, Y. Xu, J. Power Sources 267 (2014) 469-490.
- [8] H.K. Liu, Z. Guo, J. Wang, K. Konstantinov, J. Mater. Chem. 20 (2010) 10055–10057.
- [9] W.-J. Zhang, J. Power Sources 196 (2011) 13-24.
- [10] H. Kim, M. Seo, M.-H. Park, J. Cho, Angew. Chem. Int. Ed. 49 (2010) 2146-2149.
- [11] M. Armand, J.-M. Tarascon, Nature 451 (2008) 652-657.
- [12] K. Zhao, M. Pharr, L. Hartle, J.J. Vlassak, Z. Suo, J. Power Sources 218 (2012) 6–14.
- [13] X. Chen, X. Li, F. Ding, W. Xu, J. Xiao, Y. Cao, P. Meduri, J. Liu, G.L. Graff, J.-G. Zhang, Nano Lett. 12 (2012) 4124–4130.
- [14] T. Chen, J. Wu, Q. Zhang, X. Su, J. Power Sources 363 (2017) 126-144.
- [15] Z. Liu, Q. Yu, Y. Zhao, R. He, M. Xu, S. Feng, S. Li, L. Zhou, L. Mai, Chem. Soc. Rev. 48 (2019) 285–309.
- [16] X. Zhou, Z. Qi, Q. Liu, J. Tian, M. Liu, K. Dong, Z. Lei, Front. Mater. 7 (2021).
- [17] M. Khan, X. Ding, H. Zhao, Y. Wang, N. Zhang, X. Chen, J. Xu, J. Electron. Mater. (2022).
- [18] T. Wang, X. Guo, H. Duan, C. Chen, H. Pang, Chin. Chem. Lett. 31 (2020) 654–666.
- [19] K. Schulmeister, W. Mader, J. Non-Cryst. Solids 320 (2003) 143–150.
- [20] Y. Yamada, Y. Iriyama, T. Abe, Z. Ogumi, J. Electrochem. Soc. 157 (2010) A26–A30.
- [21] J.-H. Kim, C.-M. Park, H. Kim, Y.-J. Kim, H.-J. Sohn, J. Electroanal. Chem. 661 (2011) 245–249.
- [22] M. Miyachi, H. Yamamoto, H. Kawai, T. Ohta, M. Shirakata, J. Electrochem. Soc. 152 (2005) A2089–A2091.
- [23] L. Zhang, Y. Qin, Y. Liu, Q. Liu, Y. Ren, A.N. Jansen, W. Lu, J. Electrochem. Soc. 165 (2018) A2102–A2107.
- [24] F. Holtstiege, P. Bärmann, R. Nölle, M. Winter, T. Placke, Batteries 4 (2018) 4.
- [25] L. Jin, C. Shen, A. Shellikeri, Q. Wu, J. Zheng, P. Andrei, J.-G. Zhang, J.P. Zheng, Energy Environ. Sci. 13 (2020) 2341–2362.
- [26] L. Jin, C. Shen, Q. Wu, A. Shellikeri, J. Zheng, C. Zhang, J.P. Zheng, Adv. Sci. 8 (2021), 2005031.
- [27] N. Liu, L. Hu, M.T. McDowell, A. Jackson, Y. Cui, ACS Nano 5 (2011) 6487–6493.
- [28] W.M. Dose, C.S. Johnson, Curr. Opin. Electrochem. 31 (2022), 100827.
- [29] B. Huang, T. Huang, L. Wan, A. Yu, ACS Sustainable Chem. Eng. 9 (2021) 648–657.
- [30] J. Zhao, Z. Lu, N. Liu, H.-W. Lee, M.T. McDowell, Y. Cui, Nat. Commun. 5 (2014) 5088.
- [31] Z. Liu, S. Ma, X. Mu, R. Li, G. Yin, P. Zuo, ACS Appl. Mater. Interfaces 13 (2021) 11985–11994.
- [32] L. Zhang, W.M. Dose, A.D. Vu, C.S. Johnson, W. Lu, J. Power Sources 400 (2018) 549-555.
- [33] K. Park, B.-C. Yu, J.B. Goodenough, Adv. Energy Mater. 6 (2016), 1502534-n/a.
- [34] Y. Sun, Y. Li, J. Sun, Y. Li, A. Pei, Y. Cui, Energy Storage Mater. 6 (2017) 119–124.
- [35] I.W. Seong, K.T. Kim, W.Y. Yoon, J. Power Sources 189 (2009) 511-514.
- [36] J. Zhao, H.-W. Lee, J. Sun, K. Yan, Y. Liu, W. Liu, Z. Lu, D. Lin, G. Zhou, Y. Cui, Proc. Natl. Acad. Sci. USA 113 (2016) 7408.
- [37] I.W. Seong, W.Y. Yoon, J. Power Sources 195 (2010) 6143-6147.
- [38] I.W. Seong, J.H. Yom, S.M. Cho, W.Y. Yoon, in: 3rd Asia-Pacific World Congress on Computer Science and Engineering (APWC on CSE), Denarau Island, 2016, pp. 78–83. Fiji.
- [39] A. Veluchamy, C.-H. Doh, D.-H. Kim, J.-H. Lee, D.-J. Lee, K.-H. Ha, H.-M. Shin, B.-S. Jin, H.-S. Kim, S.-I. Moon, C.-W. Park, J. Power Sources 188 (2009) 574–577.
- [40] J.H. Yom, S.W. Hwang, S.M. Cho, W.Y. Yoon, J. Power Sources 311 (2016) 159–166.
- [41] L. Xie, H. Liu, S. Lin, X. Yang, M. Qi, L. Zhu, Y. Guo, G. Guo, RSC Adv. 9 (2019) 11369–11376.
- [42] Y. Zhang, G. Guo, C. Chen, Y. Jiao, T. Li, X. Chen, Y. Yang, D. Yang, A. Dong, J. Power Sources 426 (2019) 116–123.

- [43] J.-H. Kim, H.-J. Sohn, H. Kim, G. Jeong, W. Choi, J. Power Sources 170 (2007) 456-459
- C.-H. Doh, C.-W. Park, H.-M. Shin, D.-H. Kim, Y.-D. Chung, S.-I. Moon, B.-S. Jin, H.-S. Kim, A. Veluchamy, J. Power Sources 179 (2008) 367-370.
- [45] L. Hu, W. Xia, R. Tang, R. Hu, L. Ouyang, T. Sun, H. Wang, Front. Chem. 8 (2020).
- [46] D.J. Lee, M.-H. Ryou, J.-N. Lee, B.G. Kim, Y.M. Lee, H.-W. Kim, B.-S. Kong, J.-K. Park, J.W. Choi, Electrochem. Commun. 34 (2013) 98-101.
- [47] J. Wang, M. Zhou, F. Wu, S. Chen, Adv. Mater. Res. 1092-1093 (2015) 185-190.
- [48] X. Yuan, H. Xin, X. Qin, X. Li, Y. Liu, H. Guo, Electrochim. Acta 155 (2015) 251-256.
- K.W. Kim, H. Park, J.G. Lee, J. Kim, Y.-U. Kim, J.H. Ryu, J.J. Kim, S.M. Oh, Electrochim. Acta 103 (2013) 226-230.
- [50] J. Zhang, J. Zhang, T. Bao, X. Xie, B. Xia, J. Power Sources 348 (2017) 16-20.
- [51] T. Xu, J. Zhang, C. Yang, H. Luo, B. Xia, X. Xie, J. Alloys Compd. 738 (2018)
- J. Woo, S.-H. Baek, J.-S. Park, Y.-M. Jeong, J.H. Kim, J. Power Sources 299 (2015) 25-31.
- [53] F. Song, X. Yang, S. Zhang, L.-L. Zhang, Z. Wen, Ceram. Int. 44 (2018) 18509-18515.
- F. Cheng, G. Wang, Z. Sun, Y. Yu, F. Huang, C. Gong, H. Liu, G. Zheng, C. Qin, S. Wen, Ceram. Int. 43 (2017) 4309-4313.
- [55] J. Yang, Y. Takeda, N. Imanishi, C. Capiglia, J.Y. Xie, O. Yamamoto, Solid State Ionics 152-153 (2002) 125-129.
- G. Lener, M. Otero, D.E. Barraco, E.P.M. Leiva, Electrochim. Acta 259 (2018) 1053-1058.
- [57] Y. Wang, K. Xie, X. Guo, W. Zhou, G. Song, S. Cheng, New J. Chem. 40 (2016)
- [58] J.E. Entwistle, S.G. Booth, D.S. Keeble, F. Ayub, M. Yan, S.A. Corr, D.J. Cumming, S.V. Patwardhan, Adv. Energy Mater. 10 (2020), 2001826.
- [59] J. Tu, Y. Yuan, P. Zhan, H. Jiao, X. Wang, H. Zhu, S. Jiao, J. Phys. Chem. C 118 (2014) 7357-7362.
- [60] X. Wu, Z.-q. Shi, C.-y. Wang, J. Jin, J. Electroanal. Chem. 746 (2015) 62-67.
- [61] G. Lener, A.A. Garcia-Blanco, O. Furlong, M. Nazzarro, K. Sapag, D.E. Barraco, E. P.M. Leiva, Electrochim. Acta 279 (2018) 289-300.
- [62] X. Yang, H. Huang, Z. Li, M. Zhong, G. Zhang, D. Wu, Carbon 77 (2014) 275-280.
- [63] C.-C. Yang, J.-Y. Shih, M.-Y. Wu, Energy Proc. 61 (2014) 1428-1433.
- [64] J. Cui, J. Yang, J. Man, S. Li, J. Yin, L. Ma, W. He, J. Sun, J. Hu, Electrochim. Acta 300 (2019) 470–481.
- H.-H. Li, X.-L. Wu, H.-Z. Sun, K. Wang, C.-Y. Fan, L.-L. Zhang, F.-M. Yang, J.-P. Zhang, J. Phys. Chem. C 119 (2015) 3495-3501.
- J. Meng, Y. Cao, Y. Suo, Y. Liu, J. Zhang, X. Zheng, Electrochim. Acta 176 (2015) [66] 1001-1009.
- [67] Y. Zhao, Z. Liu, Y. Zhang, A. Mentbayeva, X. Wang, M.Y. Maximov, B. Liu, Z. Bakenov, F. Yin, Nanoscale Res. Lett. 12 (2017) 459.
- T681 L.-h. Yin, M.-b. Wu, Y.-p. Li, G.-l. Wu, Y.-k. Wang, Y. Wang, N. Carbon Mater. 32 (2017) 311-318.
- Γ**6**91 H. Wang, P. Wu, M. Ou, L. Si, Y. Tang, Y. Zhou, T. Lu, Chemelectrochem 2 (2015) 508-511.
- X. Cao, X. Chuan, R.C. Massé, D. Huang, S. Li, G. Cao, J. Mater. Chem. 3 (2015) [70] 22739-22749
- [71] Z. Gu, X. Xia, C. Liu, X. Hu, Y. Chen, Z. Wang, H. Liu, J. Alloys Compd. 757 (2018) 265-272.
- [72] S. Hao, Z. Wang, L. Chen, Mater. Des. 111 (2016) 616-621.
- M. Li, J. Li, K. Li, Y. Zhao, Y. Zhang, D. Gosselink, P. Chen, J. Power Sources 240 [73] (2013) 659-666.
- Y. Yao, Y. Li, C. Li, J. Zhou, Q. Wu, Y.-Z. Zheng, J. Wu, Z. Zhou, H. Ding, X. Tao, ChemistrySelect 5 (2020) 5198-5204.
- [75] Y. Wang, W. Zhou, L. Zhang, G. Song, S. Cheng, RSC Adv. 5 (2015) 63012–63016.
- [76] S.-S. Lee, C.-M. Park, Electrochim. Acta 284 (2018) 220-225.
- B. Guo, J. Shu, Z. Wang, H. Yang, L. Shi, Y. Liu, L. Chen, Electrochem. Commun. [77] 10 (2008) 1876-1878.
- [78] Y. Yao, J. Zhang, L. Xue, T. Huang, A. Yu, J. Power Sources 196 (2011) 10240-10243.
- [79] H. Xia, Z. Yin, F. Zheng, Y. Zhang, Mater. Lett. 205 (2017) 83-86.
- [80] M.R. Babaa, A. Moldabayeva, M. Karim, A. Zhexembekova, Y. Zhang, Z. Bakenov, A. Molkenova, I. Taniguchi, Mater. Today Proc. 4 (2017) 4542-4547.
- [81] P. Lv, H. Zhao, J. Wang, X. Liu, T. Zhang, Q. Xia, J. Power Sources 237 (2013) 291-294.
- [82] Z. Yuan, N. Zhao, C. Shi, E. Liu, C. He, F. He, Chem. Phys. Lett. 651 (2016) 19-23.
- M. Sasidharan, D. Liu, N. Gunawardhana, M. Yoshio, K. Nakashima, J. Mater. [83] Chem. 21 (2011) 13881-13888.
- M. Sasidharan, K. Nakashima, N. Gunawardhana, T. Yokoi, M. Ito, M. Inoue, S.i. Yusa, M. Yoshio, T. Tatsumi, Nanoscale 3 (2011) 4768-4773.
- [85] X. Ma, Z. Wei, H. Han, X. Wang, K. Cui, L. Yang, Chem. Eng. J. 323 (2017) 252-259
- [86] T. Xiao, W. Zhang, T. Xu, J. Wu, M. Wei, Electrochim. Acta 306 (2019) 106-112.
- [87] J.-Y. Kim, D.T. Nguyen, J.-S. Kang, S.-W. Song, J. Alloys Compd. 633 (2015) 92-96.

- [88] X. Cao, X. Chuan, S. Li, D. Huang, G. Cao, Part. Part. Syst. Char. 33 (2016) 110-117.
- 1981 X. Liu, Y. Chen, H. Liu, Z.-Q. Liu, J. Mater. Sci. Technol. 33 (2017) 239-245.
- [90] M. Jiao, K. Liu, Z. Shi, C. Wang, Chemelectrochem 4 (2017) 542-549.
- [91] Y. Jiang, D. Mu, S. Chen, B. Wu, Z. Zhao, Y. Wu, Z. Ding, F. Wu, J. Alloys Compd. 744 (2018) 7–14.
- Z. Favors, W. Wang, H.H. Bay, A. George, M. Ozkan, C.S. Ozkan, Sci. Rep. 4 (2014).
- [93] N. Yan, F. Wang, H. Zhong, Y. Li, Y. Wang, L. Hu, Q. Chen, Sci. Rep. 3 (2013).
- [94] H.J. Kim, J.H. Choi, J.W. Choi, Nano Convergence 4 (2017) 24.
- W.-S. Chang, C.-M. Park, J.-H. Kim, Y.-U. Kim, G. Jeong, H.-J. Sohn, Energy Environ. Sci. 5 (2012) 6895–6899.
- [96] Q. Sun, B. Zhang, Z.-W. Fu, Appl. Surf. Sci. 254 (2008) 3774-3779.
- C. Liang, C. Zhou, Z. Chen, Y. Gan, Y. Xia, H. Huang, X. Tao, J. Zhang, W.J. I. Zhang, Ionics 24 (2018) 2233–2239.
- Y. Feng, X. Liu, L. Liu, Z. Zhang, Y. Teng, D. Yu, J. Sui, X. Wang, ChemistrySelect 3 (2018) 10338–10344.
- L. Wang, J. Xue, B. Gao, P. Gao, C. Mou, J. Li, RSC Adv. 4 (2014) 64744-64746.
- [100] J. Cui, F. Cheng, J. Lin, J. Yang, K. Jiang, Z. Wen, J. Sun, Powder Technol. 311 (2017) 1-8.
- [101] C. Chaikawang, R. Hongthong, S. Kaewmala, S. Pongha, Y. Kanapan, N. Meethong, Mater. Today Proc. 5 (2018) 13989-13994.
- [102] M. Jiao, Y. Wang, C. Ye, C. Wang, W. Zhang, C. Liang, J. Alloys Compd. 842 (2020), 155774.
- [103] Z. Long, R. Fu, J. Ji, Z. Feng, Z. Liu, ChemNanoMat 6 (2020) 1127-1135.
- [104] J. Zhang, C. Zhang, Z. Liu, J. Zheng, Y. Zuo, C. Xue, C. Li, B. Cheng, J. Power Sources 339 (2017) 86-92.
- [105] B.-C. Yu, Y. Hwa, J.-H. Kim, H.-J. Sohn, Electrochim. Acta 117 (2014) 426-430.
- [106] T. Xu, Q. Wang, J. Zhang, X. Xie, B. Xia, ACS Appl. Mater. Interfaces 11 (2019) 19959-19967.
- [107] Z. Liu, Y. Zhao, R. He, W. Luo, J. Meng, Q. Yu, D. Zhao, L. Zhou, L. Mai, Energy Storage Mater. 19 (2019) 299-305.
- [108] J. Wang, H. Zhao, J. He, C. Wang, J. Wang, J. Power Sources 196 (2011) 4811–4815.
- [109] M. Han, J. Yu, J. Power Sources 414 (2019) 435-443.
- [110] Z. Liu, D. Guan, Q. Yu, L. Xu, Z. Zhuang, T. Zhu, D. Zhao, L. Zhou, L. Mai, Energy Storage Mater. 13 (2018) 112-118.
- [111] H. Cui, K. Chen, Y. Shen, Z. Wang, Int. J. Electrochem. Sci. 13 (2018) 5474-5487.
- [112] M. Ashuri, Q. He, L.L. Shaw, J. Electroanal. Chem. 876 (2020), 114738.
- [113] M. Ashuri, O. He, Y. Liu, L.L. Shaw, Nano, Mater. Sci. 2 (2020) 297-308.
- [114] W. Wu, J. Shi, Y. Liang, F. Liu, Y. Peng, H. Yang, Phys. Chem. Chem. Phys. 17 (2015) 13451-13456.
- [115] L. Shi, W. Wang, A. Wang, K. Yuan, Z. Jin, Y. Yang, J. Power Sources 318 (2016) 184_191.
- [116] M. Li, Y. Zeng, Y. Ren, C. Zeng, J. Gu, X. Feng, H. He, J. Power Sources 288 (2015) 53-61.
- [117] Y. Ren, M. Li, J. Power Sources 306 (2016) 459-466.
- [118] Y. Ren, X. Wu, M. Li, Electrochim. Acta 206 (2016) 328-336.
- [119] M. Li, Y. Yu, J. Li, B. Chen, A. Konarov, P. Chen, J. Power Sources 293 (2015) 976_982
- [120] S.W. Hwang, J.K. Lee, W.Y. Yoon, J. Power Sources 244 (2013) 620–624.
- [121] W. Yang, H. Liu, Z. Ren, N. Jian, M. Gao, Y. Wu, Y. Liu, H. Pan, Adv. Mater.
- Interfac. 6 (2019), 1801631.
- [122] S.W. Hwang, W.Y. Yoon, J. Electrochem. Soc. 161 (2014) A1753-A1758. [123] B.Y. Jang, J.S. Lee, J.S. Kim, J. Nanosci. Nanotechnol. 13 (2013) 3690-3695.
- [124] M.K. Kim, B.Y. Jang, J.S. Lee, J.S. Kim, S. Nahm, J. Power Sources 244 (2013) 115-121.
- [125] L. Su, J. Xie, Y. Xu, L. Wang, Y. Wang, M. Ren, J. Alloys Compd. 663 (2016) 524-530
- [126] P. Zhang, L. Wang, J. Xie, L. Su, C.-a. Ma, J. Mater. Chem. 2 (2014) 3776–3782.
- [127] J. Kim, J. Ahn, H.Y. Kang, G.W. Lee, Key Eng. Mater. 777 (2018) 145–149.
- [128] J. Kim, S.Y. Kim, C.-M. Yang, G.W. Lee, Sci. Rep. 9 (2019), 13313.
- [129] P. Lv, H. Zhao, C. Gao, T. Zhang, X. Liu, Electrochim. Acta 152 (2015) 345–351.
- [130] Y. Ju, J.A. Tang, K. Zhu, Y. Meng, C. Wang, G. Chen, Y. Wei, Y. Gao, Electrochim. Acta 191 (2016) 411-416.
- [131] J. Cui, Y. Cui, S. Li, H. Sun, Z. Wen, J. Sun, ACS Appl. Mater. Interfaces 8 (2016) 30239-30247
- W. Wu, M. Wang, R. Wang, D. Xu, H. Zeng, C. Wang, Y. Cao, Y. Deng, J. Power Sources 407 (2018) 112-122.
- [133] F. Li, C. Deng, X. Liu, Y. Ding, J. Peng, ChemistrySelect 4 (2019) 8614-8620.
- [134] A. Guerfi, P. Charest, M. Dontigny, J. Trottier, M. Lagacé, P. Hovington, A. Vijh, K. Zaghib, J. Power Sources 196 (2011) 5667-5673.
- [135] J. Park, S.S. Park, Y.S. Won, Electrochim. Acta 107 (2013) 467-472.
- [136] K. Lee, S. Lim, N. Go, J. Kim, J. Mun, T.-H. Kim, Sci. Rep. 8 (2018), 11322.
- [137] M. Luo, M.-T.F. Rodrigues, L.L. Shaw, D.P. Abraham, ACS Appl. Energy Mater. 5 (2022) 5513-5518.
- Y. Han, X. Liu, Z. Lu, Appl. Sci. 8 (2018) 1245.
- C. Gao, H. Zhao, P. Lv, C. Wang, J. Wang, T. Zhang, Q. Xia, J. Electrochem. Soc. 161 (2014) A2216-A2221.